

A Criterion for Multivariate Regionalization of Spatial Data

Ranadeep Daw^{*1}, Christopher K. Wikle², Jonathan R. Bradley³, and Scott H. Holan^{2,4}

¹Division of Translational Toxicology, National Institute of Environmental Health Sciences, Durham, NC, USA

²Department of Statistics, University of Missouri, Columbia, MO, USA

³Department of Statistics, Florida State University, Tallahassee, FL, USA

⁴Research and Methodology Directorate, U.S. Census Bureau, Washington, D.C., USA

December 22, 2023

Abstract

The modifiable areal unit problem in geography or the change-of-support (COS) problem in statistics demonstrates that the interpretation of spatial (or spatio-temporal) data analysis is affected by the choice of resolutions or geographical units used in the study. The ecological fallacy is one famous example of this phenomenon. Here we investigate the ecological fallacy associated with the COS problem for multivariate spatial data with the goal of providing a data-driven discretization criterion for the domain of interest that minimizes aggregation errors. The discretization is based on a novel multiscale metric, called the Multivariate Criterion for Aggregation Error (MVCAGE). Such multi-scale representations of an underlying multivariate process are often formulated in terms of basis expansions. We show that a particularly useful basis expansion in this context is the multivariate Karhunen-Loève expansion (MKLE). We use the MKLE to build the MVCAGE loss function and use it within the framework of spatial clustering algorithms to perform optimal spatial aggregation. We demonstrate the effectiveness of our approach through simulation and through regionalization of county-level income and hospital quality data over the United States and prediction of ocean color in the coastal Gulf of Alaska.

Keywords: Spatial aggregation, basis function models, multiscale data, Karhunen-Loève expansions.

^{*}Corresponding author. Email: ranadeep.daw@nih.gov

1 Introduction

Multivariate spatial data analysis refers to the statistical methods and techniques used to analyze multivariate data correlated across locations and variables. Spatial data analysis deals with observations that are dependent on each other based on their spatial locations. The multivariate spatial analysis extends this notion to include multiple observations that are not only correlated via their locations but also demonstrate inter-correlation structure among the multiple univariate variables. Hence, multivariate spatial analysis provides a more comprehensive understanding of the system under study, allowing for the identification of complex spatial patterns and relationships between variables that would be missed by univariate analysis. By capturing the cross-dependence between variables, multivariate analysis can provide more accurate predictions and facilitate better decision-making in a wide range of fields such as urban planning, public health, and environmental management.

Naturally, multivariate spatial data analysis finds its applications in various fields such as geography (Fotheringham et al., 2000), epidemiology (Elliot et al., 2000), ecology (Borcard et al., 1992), and public health (Lawson and Clark, 2002). Some key contributions in the development of this topic include Ver Hoef and Cressie (1993), Ver Hoef and Barry (1998), Gelfand (2021), Cressie and Wikle (2011), Cressie and Zammit-Mangion (2016). A recent survey on visualization of such multivariate data is given by He et al. (2019). Multivariate Gaussian processes are also useful in this context and have seen recent advancement among both the statistical and machine learning communities (e.g., see Rasmussen and Williams, 2006; Chen et al., 2023). These methods often model covariance matrices using a joint multivariate covariance kernel. See Genton and Kleiber (2015) for a review of joint covariance kernels.

There are several challenges in multivariate spatial analysis compared to the univariate case. For example, visualization and interpretation of multivariate data are common issues among re-

searchers. Dimensionality is another issue in multivariate analysis, which affects the associated storage and computational costs and may also lead to data sparsity and the curse of dimensionality. Another challenging aspect in multivariate spatial analysis arises from the complex dependence structure among the variables and the spatial locations. The storage (computation) cost of the joint covariance matrix of multivariate spatial data is of quadratic (cubic) order of the number of variables and locations. Mathematically, the covariance function is vector-valued, leading to matrix-valued reproducing kernels and vector-valued eigenfunctions. Although in many cases there are straightforward extensions from the univariate methods to accommodate multivariate spatial data, many additional challenges arise in practical applications, such as singularity, instability, and numerical accuracy in computation. In this manuscript, we review a procedure to build these cross-covariance matrices starting from univariate covariance functions and their eigenpairs.

Another important application of spatial analysis is spatial regionalization, which involves dividing a study area into regions based on similarities or dissimilarities between variables. Univariate regionalization has been widely studied and used in geography and other disciplines to identify regions with similar values of a single variable (Openshaw, 1984; Anselin, 1988; Bailey and Gatrell, 1995). In the context of multivariate data, separate regionalization models based on the individual univariate processes lead to suboptimal solutions since it ignores the cross-covariance information between the univariate processes. This supports the study of multivariate spatial regionalization, which looks to identify regions that exhibit similar patterns across multiple variables. This approach has been applied in a variety of fields, including ecology, hydrology, and land use planning, to identify regions with similar ecological or land use characteristics, and to inform spatial decision-making (Tatem et al., 2003; Peña-Angulo et al., 2022).

Univariate spatial regionalization techniques include common clustering techniques and many other methods specific to spatial regionalization. Common clustering techniques include k -means clustering (MacQueen, 1967), hierarchical agglomerative clustering (Sneath and Sokal, 1962; Ward Jr,

1963), fuzzy clustering (Bezdek, 1981), decision trees (Quinlan, 1986), and others. Other approaches specific to spatial regionalization include expert-based methods (Mennis, 2002), the Max- p method (Duque et al., 2012), minimum spanning trees (Assunção et al., 2006), genetic optimization (Bacao et al., 2005), and others. Each methodology aims to partition the space into regions similar to an ANOVA-like partition, by maximizing within-region similarity while minimizing similarity between regions. The Max- p method uses a hierarchical clustering approach to partition regions into sub-regions based on the maximum probability of similarity. In contrast, minimum spanning trees consider a minimum spatial connectivity graph with the lowest cost, then remove its edges to produce regions.

The Modifiable Areal Unit Problem (MAUP) is a common phenomenon that often arises in spatial regionalization or aggregation methods. It is a manifestation of Simpson’s paradox, i.e., spatial data corresponding to the two resolutions – original and aggregate level – may lead to contradictory inferences about the underlying process. This is also known as the ecological fallacy and is associated with the spatial change-of-support (COS) problem. MAUP or the ecological fallacy has been extensively studied in geospatial and ecological studies (e.g., see Openshaw, 1979; Gotway and Young, 2002; Banerjee et al., 2004; Wikle and Berliner, 2005; Robinson, 2009; Bradley et al., 2017; Zhou and Bradley, 2023). However, there has been a relatively less research aimed at quantifying and minimizing MAUP in spatial COS. The Criterion for Aggregation Error (CAGE), introduced by Bradley et al. (2017), addresses this issue by computing a statistic that measures the spatial aggregation error incurred through COS for multi-scale spatial processes. The CAGE statistic links both the spatial processes and their covariance matrices using the Karhunen-Loève expansion (KLE) of a data-driven covariance kernel and computes the average distance between two different resolution-level eigenfunctions (i.e., original and aggregated) inside these regions. Minimizing CAGE is then the same as finding a partition such that the eigenfunctions are homogeneous inside the partitions. In this way, CAGE quantifies and then helps minimize the ecological fallacy

or MAUP in spatial COS.

In this paper, we broaden the application of the CAGE method to encompass multivariate spatial data. This is a promising and evolving research field, considering the prevalence of multivariate information and its implications for multivariate spatial regionalization. We introduce a novel metric, namely MVCAGE, to account for the amount of ecological fallacy or MAUP in the multivariate context. MVCAGE utilizes the multivariate equivalent of the KLE (see Daw et al., 2022, for a review of multivariate KLE), where multivariate eigenfunctions are used as the optimal feature expansion method for the multivariate spatial processes. Therefore, given a choice of the number of possible regions, MVCAGE yields an optimal regionalization, i.e., the one with the minimum amount of ecological fallacy. Another advantage of using multivariate eigenfunctions is that both the spatial process and its covariance matrix are direct consequences of these. Therefore, partitioning based on these eigenfunctions leads to homogeneity in both the aggregated data and the covariance matrix. We present Propositions 2.4 and 2.5 to show the rationale behind the MVCAGE criterion and, to demonstrate our methodology, we consider simulation and application of our approach to regionalization and prediction.

The manuscript is structured as follows. Section 2 provides background on multivariate KLE and data-driven computation. Section 3 presents our methodology on how to integrate these techniques. Section 4 showcases simulation along with regionalization through regionalization of county-level income and hospital quality data over the United States. Section 5 discusses the advantages and limitations of our approach, and puts forward ideas for future research. We also provide additional Supplemental Materials which include the proof of constructions of the proposals, technical details of computation, and an additional application of bivariate regionalization using a ocean color dataset.

2 Multivariate Karhunen-Loève expansion and MVCAGE

In this section, we present the mathematical notation used in this paper and the background of the multivariate KLE. We then proceed with motivating the idea behind the multivariate CAGE from the multivariate KLE.

2.1 Notation

Let $\mathcal{S} \in \mathbb{R}^d$ denote the spatial domain under study, where d is often 1, 2, or 3 for geospatial problems. We consider a set of N univariate spatial random variables $\{Z_1(\mathbf{s}), \dots, Z_N(\mathbf{s})\} : \mathcal{S} \rightarrow \mathbb{R}$. Corresponding to each $Z_j(\mathbf{s})$, we define the latent, noise-free, zero-mean, continuous spatial process by $Y_j(\mathbf{s}) : \mathcal{S} \rightarrow \mathbb{R}, j = 1, \dots, N$. We denote the mean function of $Z_j(\mathbf{s})$ as $\mu_j(\mathbf{s})$, and also define a set of error processes $\epsilon_j(\mathbf{s}) : \mathcal{S} \rightarrow \mathbb{R}$ with zero-mean and finite variances for $j = 1, \dots, N$.

In the multivariate context, we use lower-case bold font to denote the respective multivariate versions. For example, $\mathbf{z}(\mathbf{s}) = (Z_1(\mathbf{s}), \dots, Z_N(\mathbf{s}))^\top \in \mathbb{R}^N$ denotes the multivariate spatial observations, $\mathbf{y}(\mathbf{s}) = (Y_1(\mathbf{s}), \dots, Y_N(\mathbf{s}))^\top \in \mathbb{R}^N$ shows the corresponding vector valued latent process, and $\boldsymbol{\mu}(\mathbf{s}) = (\mu_1(\mathbf{s}), \dots, \mu_N(\mathbf{s}))^\top \in \mathbb{R}^N$ is the vector-valued mean function. We assume that $\mathbf{z}(\mathbf{s})$ is observed at n locations denoted by $\mathbf{S} = \{\mathbf{s}_1, \dots, \mathbf{s}_n\}$. We allow for missing observations, i.e., we do not require each Z_j to be observed at every $\mathbf{s}_k \in \mathbf{S}$. The math-bold symbols (e.g., \mathbf{Z}, \mathbf{Y}) denote the data matrices corresponding to the bold-faced symbols. For example, the $n \times N$ matrix \mathbf{Z} is the observed data, where the j, k -th element of \mathbf{Z} is the realization of the k -th univariate variable Z_k at location \mathbf{s}_j (i.e., $Z_k(\mathbf{s}_j)$).

Next, we introduce covariance functions and covariance matrices. Given two spatial locations \mathbf{s} and \mathbf{r} , the positive-definite covariance function of the univariate process $Y_j(\cdot)$ is denoted as $C_{jj}(\mathbf{s}, \mathbf{r}) = \text{cov}[Y_j(\mathbf{s}), Y_j(\mathbf{r})] : \mathcal{S} \times \mathcal{S} \rightarrow \mathbb{R}$. The corresponding covariance matrix is the evaluation of C_{jj} at $\mathbf{S} \times \mathbf{S} = \{(\mathbf{s}_k, \mathbf{s}_\ell) : k, \ell = 1, \dots, n\}$; is denoted by $\mathbf{C}_{jj} \in \mathbb{R}^{n \times n}$, and its k, ℓ -th element

is given by $\text{cov} [Y_j(\mathbf{s}_k), Y_j(\mathbf{s}_\ell)]$. The inter-variable cross-covariance functions are of a similar form given by $C_{ij}(\mathbf{s}, \mathbf{r}) = \text{cov} [Y_i(\mathbf{s}), Y_j(\mathbf{r})]$. We similarly denote the cross-covariance matrices (i.e., evaluations of C_{ij} over $\mathcal{S} \times \mathcal{S}$) as $\mathbf{C}_{ij} \in \mathbb{R}^{n \times n}$. The multivariate covariance function of the multivariate spatial process \mathbf{y} is denoted by $\mathbb{C}(\cdot, \cdot) : \mathcal{S} \times \mathcal{S} \rightarrow \mathbb{R}^{N \times N}$. We similarly denote the multivariate joint covariance matrix by \mathbf{C} . It is easy to see that \mathbf{C} is a block matrix of order $\mathbb{R}^{nN \times nN}$ with blocks $\mathbf{C}_{ij} \in \mathbb{R}^{n \times n}$; $i, j = 1, \dots, N$. Now, for the j -th univariate covariance function C_{jj} , we denote its k -th eigenfunction as $\psi_{jk}(\mathbf{s}) : \mathcal{S} \rightarrow \mathbb{R}$ and the corresponding eigenvalue is denoted by λ_{jk} for $k = 1, 2, \dots, \infty$.

To consider spatial data at different resolutions, we often use the terms “point-level” and “areal” (or area-level). Point-level or point-referenced spatial data refers to random variables whose arguments are the points from \mathcal{S} , i.e., subsets of \mathcal{S} with Lebesgue measure zero. Alternatively, areal data denotes spatial random variables that take non-zero Lebesgue measurable subsets of \mathcal{S} as arguments. We use bold lowercase vectors (e.g., \mathbf{s}, \mathbf{r}) to denote the point locations and calligraphic capital letters (e.g., $\mathcal{A}, \mathcal{B}, \mathcal{S}$) to denote areal units. Area-level random variables are denoted by a superscript “ A ”. For example, $\mathbf{z}^A(\mathcal{A}) = (Z_1^A(\mathcal{A}), \dots, Z_N^A(\mathcal{A}))^\top$ and $\mathbf{y}^A(\mathcal{A}) = (Y_1^A(\mathcal{A}), \dots, Y_N^A(\mathcal{A}))^\top$ are the multivariate areal data and process vectors. Without any superscript, the random variables (e.g., $Z_j(\mathbf{s}), \mathbf{y}_k(\mathbf{s})$) denote the point-level versions. Note that the area of \mathcal{S} can be expressed in terms of the point-level support as $|\mathcal{S}| = \int_{\mathbf{s} \in \mathcal{S}} d\mathbf{s}$ and areal support as $\mathcal{S} = \sum_{\mathcal{A}_j \in \tilde{\mathcal{A}}} |\mathcal{A}_j|$ where $\tilde{\mathcal{A}} = \{\mathcal{A}_1, \mathcal{A}_2, \dots, \mathcal{A}_M : \cup_j \mathcal{A}_j = \mathcal{S}, \mathcal{A}_i \cap \mathcal{A}_j = \emptyset\}$.

It is important to note that we may need to deal with multiple area-level resolutions. For example, one may want to join neighboring census block-groups to create a census tract or county. In such cases, we use \mathcal{B} to represent the areal units at the higher resolution and \mathcal{A} to denote the aggregated lower resolution. In this example, $Z_j^{\mathcal{B}}$ corresponds to a variable at the census block-group level, and $Z_j^{\mathcal{A}}$ are the created census tracts or counties.

2.2 Univariate Karhunen-Loève Expansion

For each of the latent univariate processes Y_j with covariance function C_{jj} , there exists a KLE of the following form (Karhunen, 1947; Loève, 1945; Cressie and Wikle, 2011)

$$Y_j(\mathbf{s}) = \sum_{k=1}^{\infty} \alpha_{jk} \psi_{jk}(\mathbf{s}). \quad (1)$$

Here, the expansion functions $\psi_{jk}(\mathbf{s}) : \mathcal{S} \rightarrow \mathbb{R}$ are deterministic, spatially-varying functions, and the expansion coefficients α_{jk} 's are mean-zero, uncorrelated random variables with respective variances $\lambda_{j1} \geq \lambda_{j2} \geq \dots \geq 0$. The KLE is the consequence of Mercer's theorem (Aronszajn, 1950), which provides the connection between a set of dependent random variables and their covariance functions. Together with Mercer's theorem, the KLE yields the following properties:

$$\begin{aligned} \text{(P1:)} \quad C_{jj}(\mathbf{s}, \mathbf{r}) &= \sum_{k=1}^{\infty} \lambda_{jk} \psi_{jk}(\mathbf{s}) \psi_{jk}(\mathbf{r}), \\ \text{(P2:)} \quad \int_{\mathbf{s}} \psi_{jk}(\mathbf{s}) \psi_{j\ell}(\mathbf{s}) d\mathbf{s} &= \delta_{k\ell} \quad (\text{i.e., } 1 \text{ if } k = \ell, 0 \text{ otherwise}), \\ \text{(P3:)} \quad \mathbb{E}[\alpha_{jk}] &= 0, \quad \text{cov}[\alpha_{jk}, \alpha_{j\ell}] = \lambda_{jk} \delta_{k\ell}, \\ \text{(P4:)} \quad \alpha_{jk} &= \int_{\mathbf{s}} Y_j(\mathbf{s}) \psi_{jk}(\mathbf{s}) d\mathbf{s}, \end{aligned}$$

where $\delta_{k\ell}$ represents the Dirac delta function. The above properties demonstrate the bi-orthogonal property of the KLE, which means that the KLE uses both the uncorrelated expansion coefficients and orthonormal eigenfunctions in the expansion in (1).

The eigenvalues $\lambda_{j1}, \lambda_{j2}, \dots$ are non-negative for any positive-definite covariance function and monotonically decrease to zero. Since $\text{var}(\alpha_{jk}) = \lambda_{jk} \xrightarrow{k \rightarrow \infty} 0$, the random variables (α_{jk}) also shrink to the Dirac zero distribution. Therefore, this provides the rationale behind the truncation of the infinite sum in Equation (1) at some finite number M_j . Given such a cutoff value M_j , the truncated KLE satisfies the optimal \mathcal{L}_2 approximation criterion, i.e., $\tilde{Y}_j(\mathbf{s}) = \sum_{k=1}^{M_j} \alpha_{jk} \psi_{jk}(\mathbf{s})$ has minimum mean-square prediction error for $Y_j(\mathbf{s})$ among all linear expansions with M_j terms. This optimal

approximation, in addition to the bi-orthogonality criterion, justifies using the KLE as an optimal linear expansion in analyzing dependent processes.

Additional consequences of the KLE properties include the following. If \check{Y}_j has the same distribution as Y_j , the KLE of \check{Y}_j yields the same eigenpairs as Y_j ; i.e., $\check{Y}_j = \sum_{k=1}^{\infty} \check{\alpha}_{jk} \psi_{jk}$. Each expansion coefficient $\check{\alpha}_{jk}$ then follows the same distribution as α_{jk} . Therefore, fixing α_{jk} , the eigenfunctions can be interpreted as the \mathcal{L}_2 -optimal spatially varying features, which motivated the development of the CAGE criterion in Bradley et al. (2017). Another interesting consequence of the KLE properties is that when Y_j are Gaussian processes, the expansion coefficients α_{jk} are uncorrelated normal random variables, and hence, also independent.

Remark 2.1. Note that the choice of M_j is often data dependent and usually chosen by the practitioner. There are some standard techniques to find a reasonable number of eigenpairs, such as scree plots, percentage of variance explained, and pre-fixed cutoff value, etc. In practice, the final choice of M_j should include a sensitivity analysis.

2.3 Multivariate KLE

In this section, we discuss the extension of the KLE to multivariate domains to accommodate multivariate spatial processes. This is fundamental to our multivariate CAGE criterion. To describe the multivariate KLE (MKLE), we consider a multivariate spatial process $\mathbf{y}(\mathbf{s}) : \mathcal{S} \rightarrow \mathbb{R}_N$ with mean $\mathbf{0}$ and finite covariance function $\mathbb{C}(\mathbf{s}, \mathbf{r})$ and introduce the multivariate version of Mercer's theorem as follows:

$$\begin{aligned}
 \text{(P1:)} \quad \mathbb{C}(\mathbf{s}, \mathbf{r}) &= \sum_{k=1}^{\infty} \lambda_k \boldsymbol{\psi}_k(\mathbf{s}) \boldsymbol{\psi}_k(\mathbf{r})^\top, & (2) \\
 \text{(P2:)} \quad \mathbf{y}(\cdot) &= \sum_{k=1}^{\infty} \alpha_k \boldsymbol{\psi}_k(\cdot), \\
 \text{(P3:)} \quad \int_{\mathcal{S}} \boldsymbol{\psi}_k^\top(\mathbf{s}) \boldsymbol{\psi}_\ell(\mathbf{s}) d\mathbf{s} &= \delta_{k\ell},
 \end{aligned}$$

$$\text{(P4:)} \quad \mathbb{E}[\alpha_k] = 0, \text{ cov} [\alpha_k, \alpha_\ell] = \lambda_k \delta_{k\ell}.$$

Here, the expansion coefficients α_k -s are the stochastic component of the MKLE and the corresponding multivariate eigenfunctions $\boldsymbol{\psi}_k$ are the deterministic expansion functions. Each α_k is a univariate mean-zero random variable with variance λ_k , the k -th eigenvalue of the multivariate covariance function $\mathbb{C}(\cdot, \cdot) \rightarrow \mathbb{R}^{N \times N}$. Note that $\mathbb{C}(\mathbf{s}, \mathbf{r})$ is matrix-valued, symmetric, and positive-definite with monotonically shrinking eigenvalues $\lambda_1 \geq \lambda_2 \geq \dots \geq 0$ and multivariate orthonormal eigenfunctions $\boldsymbol{\psi}_k(\mathbf{s}) : \mathcal{S} \rightarrow \mathbb{R}^N, k = 1, 2, \dots$ of \mathbb{C} as in the above. Similar to the univariate case, α_k -s shrink to the Dirac zero distribution as $k \rightarrow \infty$.

Although the above formulation is intuitive from the univariate KLE, the challenge lies in defining the multivariate covariance functions and the corresponding vector-valued eigenfunctions $\boldsymbol{\psi}_k$. In practice, one should be careful in maintaining the positive-definiteness of \mathbb{C} . The vector-valued eigenfunctions and their orthonormality constraints can also be difficult to work with. As such, it is easier to build these multivariate eigenfunctions from their process-specific univariate KLEs. We provide a brief description of this procedure next.

We use Proposition 5 from Happ and Greven (2018) that establishes the bijective relationship between a multivariate KLE and its process-specific univariate KLEs. Suppose we have the univariate KLEs in the form of (1) for all the N univariate processes. For the j -th process, the expansion coefficients α_{jk} and $\alpha_{j\ell}$ are uncorrelated for $k \neq \ell$. However, for two different processes i and j , the expansion coefficients α_{ik} and $\alpha_{j\ell}$ are correlated. We decorrelate the expansion coefficients in the following manner. Define \mathbf{K}_{ij} as the $M_i \times M_j$ matrix with k, ℓ -th element given by $K_{k\ell}^{ij} = \text{cov} [\alpha_{ik}, \alpha_{j\ell}]$. From the Fredholm integral equations, we have the following (Cho et al., 2013)

$$K_{k\ell}^{ij} = \int_{\mathcal{S}} \int_{\mathcal{S}} C_{ij}(\mathbf{s}, \mathbf{r}) \psi_{ik}(\mathbf{s}) \psi_{j\ell}(\mathbf{r}) d\mathbf{s} d\mathbf{r}, \quad \text{for } k, \ell = 1, \dots, n.$$

We denote \mathbf{K} as the block matrix with \mathbf{K}_{ij} as the i, j -th block. Each \mathbf{K}_{jj} is a diagonal matrix with

the eigenvalues of the j -th process as the diagonal elements. Note that \mathbf{K} is a symmetric matrix of size $\mathbb{R}^{M \times M}$, where $M = \sum_{j=1}^N M_j$. Assuming the positive definiteness of \mathbf{K} , we must compute the eigenvalues and eigenvectors of \mathbf{K} , through which we decorrelate the univariate expansion coefficients α_{jk} -s of the different univariate processes. Proposition 5 from Happ and Greven (2018) proves that the eigenvalues of \mathbf{K} are the eigenvalues for the MKLE of \mathbb{C} .

To compute the expansion coefficients and multivariate eigenfunctions, denote the k -th eigenvector of \mathbf{K} as \mathbf{e}_k , where $\mathbf{e}_k \in \mathbb{R}^M$. Each \mathbf{e}_k can be written in the blocked form with blocks $\mathbf{e}_k^1, \dots, \mathbf{e}_k^N$. If the j -th univariate truncated KLE of C_{jj} has M_j terms, the j -th block \mathbf{e}_k^j is of size M_j . Then, the j -th element of the k -th truncated MKLE and the expansion coefficients for the MKLE are given by

$$[\boldsymbol{\psi}_k]_j = (\psi_{j1}, \dots, \psi_{jM_j}) \mathbf{e}_k^j. \quad (3)$$

$$\alpha_k = \sum_{j=1}^N (\alpha_{j1}, \dots, \alpha_{jM_j}) \mathbf{e}_k^j. \quad (4)$$

The above completes the construction of the multivariate eigenfunctions from the univariate case. If the truncated KLE of Y_j has M_j terms, the vector-valued eigenfunctions are of dimension $M = \sum_{j=1}^N M_j$. Similar to the univariate case, the MKLE yields the minimum \mathcal{L}_2 error (i.e., mean-square error) among all linear expansions of \mathbf{y} with M -terms, which makes the MKLE the \mathcal{L}_2 -optimal expansion method along with the bi-orthogonality property of uncorrelated expansion coefficients and orthonormal expansion functions. We provide the proof of correctness of the above construction procedure in Appendix A.

2.4 Multivariate CAGE

Using the MKLE for dependent data, we now address the issue of the spatial COS and propose the multivariate CAGE statistic. To motivate our idea, we first look at the problem of dealing with spatial data having multiple resolutions. Consider any point-level (multivariate) spatial process

$\mathbf{y}(\mathbf{s}) : \mathcal{S} \rightarrow \mathbb{R}^N$. We define the corresponding areal-version of this variable as

$$\mathbf{y}^A(\mathcal{A}) = \frac{1}{|\mathcal{A}|} \int_{\mathbf{s} \in \mathcal{A}} \mathbf{y}(\mathbf{s}) d\mathbf{s}, \quad (5)$$

where $\mathbf{y}^A(\mathcal{A})$ are the continuous average of $\mathbf{y}(\mathbf{s})$ over an areal unit \mathcal{A} (e.g., see Cressie and Wikle, 2011). The above formulation leads to the following few propositions about the areal covariance kernel.

Proposition 2.1. The areal covariance function takes the following form:

$$\begin{aligned} \text{cov} [\mathbf{y}^A(\mathcal{A}_i), \mathbf{y}^A(\mathcal{A}_j)] &= \frac{1}{|\mathcal{A}_i|} \frac{1}{|\mathcal{A}_j|} \int_{\mathbf{s} \in \mathcal{A}_i} \int_{\mathbf{r} \in \mathcal{A}_j} \text{cov} [\mathbf{y}(\mathbf{s}), \mathbf{y}(\mathbf{r})] d\mathbf{s} d\mathbf{r} \\ &= \frac{1}{|\mathcal{A}_i|} \frac{1}{|\mathcal{A}_j|} \int_{\mathbf{s} \in \mathcal{A}_i} \int_{\mathbf{r} \in \mathcal{A}_j} \mathbf{y}(\mathbf{s}) \mathbf{y}(\mathbf{r})^\top d\mathbf{s} d\mathbf{r}. \end{aligned}$$

Proposition 2.2. Define the function $\boldsymbol{\psi}_k^A(\mathcal{A}) = \frac{1}{|\mathcal{A}|} \int_{\mathbf{s} \in \mathcal{A}} \boldsymbol{\psi}_k(\mathbf{s}) d\mathbf{s}$. Then, the areal covariance function uses these areal functions to attain an MKLE as

$$\text{cov} [\mathbf{y}^A(\mathcal{A}_i), \mathbf{y}^A(\mathcal{A}_j)] = \sum_{k=1}^{\infty} \lambda_k \boldsymbol{\psi}_k^A(\mathcal{A}_i) \boldsymbol{\psi}_k^A(\mathcal{A}_j)^\top.$$

Proposition 2.3. The area-level random variables also attain a similar expansion as

$$\mathbf{y}^A(\mathcal{A}) = \sum_{k=1}^{\infty} \alpha_k \boldsymbol{\psi}_k^A(\mathcal{A}).$$

The proofs Propositions 2.1–2.3 are included in Appendix B.

Using the above, we now propose the multivariate CAGE statistic. To mitigate the ecological fallacy in the spatial COS, Bradley et al. (2017) first proposed to minimize the distance between the point and area-level eigenfunctions. We similarly extend this in the multivariate domain to introduce the multivariate CAGE (MVCAGE) criterion as

$$\text{MVCAGE}(\mathcal{A}) = \lambda_k [\boldsymbol{\psi}_k(\mathcal{A}) - \boldsymbol{\psi}_k(\mathbf{s})]^\top [\boldsymbol{\psi}_k(\mathcal{A}) - \boldsymbol{\psi}_k(\mathbf{s})]. \quad (6)$$

Note that MVCAGE yields the weighted squared-error loss between the point-level and area-level eigenfunctions weighted by the corresponding eigenvalues. The MVCAGE criterion is motivated by

the fact that lower values of the MVCAGE statistic correspond to more similarity in the point-level and area-level eigenfunctions. Since the covariance functions and the spatial processes are direct consequences of these eigenfunctions, the lower value of the MVCAGE corresponds to a lower amount of ecological fallacy. In addition, the following two propositions strengthen the rationale behind our construction.

Proposition 2.4. For any continuous functional $\mathbf{f} : \mathbf{y} \rightarrow \mathbb{R}^K$, a necessary and sufficient condition for $\mathbf{f} \circ \mathbf{y}(\mathbf{s}) \stackrel{a.s.}{=} \mathbf{f} \circ \mathbf{y}(\mathcal{A})$, $\mathbf{s} \in \mathcal{A}$ is that $\boldsymbol{\psi}_k(\mathbf{s}) \stackrel{a.s.}{=} \boldsymbol{\psi}_k^{\mathcal{A}}(\mathcal{A})$ for all k . (Note that $\mathbf{f} \circ \mathbf{y}(\mathbf{s}) \equiv \mathbf{f}[\mathbf{y}(\mathbf{s})]$.)

Proposition 2.5. The MVCAGE criterion can also be motivated by the following ‘‘ANOVA-type’’ decomposition:

$$\begin{aligned} \text{MVCAGE}(\mathcal{A}) &= \frac{1}{|\mathcal{A}|} \text{trace } \mathbb{E}[\mathbf{y}(\mathbf{s}) - \mathbf{y}^{\mathcal{A}}(\mathcal{A})][\mathbf{y}(\mathbf{s}) - \mathbf{y}^{\mathcal{A}}(\mathcal{A})]^\top \\ &= \frac{1}{|\mathcal{A}|} \text{trace } [\text{cov}\{\mathbf{y}(\mathbf{s})\}] - \text{trace } [\text{cov}\{\mathbf{y}^{\mathcal{A}}(\mathcal{A})\}]. \end{aligned}$$

See Appendix B for the proofs Propositions 2.4 and 2.5. Importantly, Propositions 2.4 and 2.5 provide further rationale behind MVCAGE. Proposition 2.4 establishes a stronger relationship in the sense that any functional of the two eigenfunctions are equal almost surely if and only if the point-level and area-level eigenfunctions are the same almost surely. This implies that the similarity of the two eigenfunctions can aid in minimizing the MVCAGE and hence the ecological fallacy in the data. Proposition 2.5 proposes an ANOVA-type decomposition of the MVCAGE statistic, meaning that lower MVCAGE corresponds to better consistency of the data by the aggregated units.

Although we used the weighted square error loss, we can generalize the above notion by using any convex loss function for multivariate data, e.g., Manhattan loss, KL divergence, sup-norm loss etc. Under a loss function \mathcal{L} , the generalized version of MVCAGE (GMVCAGE) can be expressed

as

$$\text{GMVCAGE}(\mathcal{A}) = \frac{1}{|\mathcal{A}|} \int_{\mathbf{s} \in \mathcal{A}} \sum_{k=1}^{\infty} \mathcal{L}[\boldsymbol{\psi}_k(\mathcal{A}), \boldsymbol{\psi}_k(\mathbf{s}); \lambda_k] d\mathbf{s},$$

One can choose any problem-specific loss function here; e.g., Daw and Wikle (2022) used \mathcal{L}_1 divergence within the framework of a minimum spanning tree and then applied the \mathcal{L}_2 loss to get the final partition for a univariate CAGE example. Specifically, the \mathcal{L}_1 loss is often advantageous for outliers and robustness. Univariate CAGE in Bradley et al. (2017) used a weighted squared error loss, with the k -th eigenfunction weighted by the eigenvalue λ_k .

2.5 Discrete Approximation

In practice it is not possible to integrate the eigenfunctions $\boldsymbol{\psi}_k$ over all possible partitions since there can be an infinite number of partitions of the space. One way to proceed is to consider a Monte-Carlo approximation of the space using a grid of points (e.g., Daw and Wikle, 2022). The idea is similar to methods used in Riemann integration, decision trees, and random forests. We use a set of pseudo points $\tilde{\mathbf{s}}_1, \dots, \tilde{\mathbf{s}}_{\tilde{n}} \in \mathcal{S}$ that lie at the centroid of regular grid “boxes”. Suppose, $\{\mathcal{B}_j\}_{j=1}^{\tilde{n}}$ is such a set of rectangular grid boxes covering \mathcal{S} . One can use Monte-Carlo integration then to evaluate the areal eigenfunctions $\boldsymbol{\psi}^A(\mathcal{B}_j)$ over these grid boxes. Alternatively, similar to approximations used in Riemann integration, we can use sufficiently small grid boxes and assume that the MKLEs do not vary substantially inside these boxes. We can then approximate the areal eigenfunctions in the following manner:

$$\boldsymbol{\psi}^A(\mathcal{B}_j) = \frac{1}{|\mathcal{B}_j|} \int_{\mathcal{B}_j} \boldsymbol{\psi}(\mathbf{s}) d\mathbf{s} \approx \frac{1}{|\mathcal{B}_j|} \boldsymbol{\psi}(\tilde{\mathbf{s}}_j) \int_{\mathcal{B}_j} d\mathbf{s} = \boldsymbol{\psi}(\tilde{\mathbf{s}}_j). \quad (7)$$

where $\tilde{\mathbf{s}}_j$ is a point from \mathcal{B}_j . We can join the grid elements in (7) to form the lower-resolution areal units, i.e., $\mathcal{A}_k = \cup_{j=1}^{n_k} \mathcal{B}_{k_j}$. Similar to the above derivation, the areal eigenfunction at the aggregated areal level \mathcal{A}_k becomes the average of the eigenfunctions over the grid elements, i.e.,

$\boldsymbol{\psi}^A(\mathcal{A}_k) = \frac{1}{n_k} \sum_{j=1}^{n_k} \boldsymbol{\psi}^A(\mathcal{B}_{k_j})$. Under this approximation, the discrete approximation of MVCAGE over \mathcal{A}_k becomes

$$\text{DMVCAGE}(\mathcal{A}_k) = \frac{1}{n_k} \sum_{j=1}^{n_k} \sum_{i=1}^{\infty} \lambda_k [\boldsymbol{\psi}_i^A(\mathcal{A}_k) - \boldsymbol{\psi}_i^A(\mathcal{B}_{k_j})]^T [\boldsymbol{\psi}_i^A(\mathcal{A}_k) - \boldsymbol{\psi}_i^A(\mathcal{B}_{k_j})]. \quad (8)$$

3 Methodology for Regionalization

Here we describe our modeling and regionalization technique. We first discuss spatial clustering methods in Section 3.1. Then, choices of various multivariate spatial models are proposed in Section 3.2. Section 3.3 discusses how to compute the univariate and multivariate eigenpairs from the fitted covariance matrices. Finally, Section 3.4 proposes the complete algorithm for spatial regionalization, utilizing the modeling, MKLE computation, clustering, and regionalization.

3.1 Spatial Clustering

The primary tool behind spatial regionalization is spatial clustering. Unlike nonspatial clustering, spatial clustering needs to account for the spatial proximity of the units to identify spatially contiguous clusters. Even then, many spatial clustering algorithms cannot guarantee explicit spatial contiguity and may require additional ad-hoc techniques (see Duque et al., 2007, for a review). In the context of MVCAGE, we explored some of these choices, namely spatial k -means (Alexandrov and Kobarg, 2011), hierarchical geographical clustering (Guha et al., 1998; Chavent et al., 2018), and minimum spanning trees (Assunção et al., 2006).

We first discuss spatial k -means and hierarchical geographical clustering (HGC) approaches, which are straightforward extensions of their respective nonspatial versions. Suppose we are interested in clustering a random vector $\mathbf{y}(\cdot)$ using spatial k -means and HGC. We first create a new variable as $\boldsymbol{\mathcal{Y}}(\mathbf{s}) = (\gamma \mathbf{y}(\mathbf{s}), (1 - \gamma) \mathbf{s})$, where the hyperparameter γ balances the ratio of effects of $\mathbf{y}(\mathbf{s})$ and the spatial proximity. We apply the respective clustering algorithms (i.e., nonspatial

k -means and hierarchical clustering) on \mathcal{Y} to get the spatial clusters. Finally, units within the same cluster are joined to create a partition or regionalization of \mathcal{S} . In practice, explicitly local partitions are often obtained in an ad-hoc fashion. For example, one can carefully tune the balancing parameter γ such that only local clusters are formed. Alternatively, one can create naive partitions using the nonspatial clustering methods and then subsequently partition the clusters with non-neighboring locations into multiple smaller clusters. Although these methods come with additional concerns about these ad-hoc techniques, they are quite commonly used due to their simple interpretations and available implementations (such as Chavent et al., 2018).

Alternatively, the minimum spanning tree (MST) (Assunção et al., 2006) is a method that yields an explicitly spatial regionalization, i.e., it only allows neighboring units in a single cluster. We first use the new response variables $\mathcal{Y}(\mathbf{s})$ to form a connected graph over the spatial domain \mathcal{S} . This represents the spatial neighborhood as a connectivity graph, where only spatial neighbors are connected with each other with unique “edges”. An edge weight is used to reflect the variable under study that is being partitioned. Subsequently, edges with higher weights are removed to yield clusters, within which units share at least one neighboring unit by construction. See Daw and Wikle (2022) for a univariate spatial regionalization methodology using MST, where the CAGE loss was incorporated within the framework of the MST.

Here we use a hybrid idea of the spatial clustering techniques, borrowing the HGC method from Bradley et al. (2017) and the clustering technique in Daw et al. (2022). The MST methodology in Daw and Wikle (2022) is applied on the space of the KLE, which by construction generate explicitly local clusters. However, we found in our studies that the naive clustering algorithms, such as k -means and HGC with Ward linkage, work reasonably well to produce spatially contiguous partitions. Additionally, the HGC with Ward linkage mitigates the computational and boundary issues of the MST, which had to be mitigated in Daw et al. (2022) by imposing additional constraints. We also note that MST is a specific case of HGC with single linkage method. Since Ward linkage

has been argued to be advantageous and a reasonable choice for agglomerative clustering, here we chose the HGC with Ward clustering to generate the spatial partitions.

3.2 MKLE for Multivariate Obled-Creutin (MVOC) basis Model

So far, we have not addressed the choices of various model assumptions for the data. However, MKLE is the direct consequence of the covariance function of the underlying process, and hence we need to consider some modeling choices to estimate the covariance matrix. In principle, any choice of multivariate spatial model can be implemented, and we discuss a few possible choices.

Recall that $\mathbf{z}(\mathbf{s})$ and $\mathbf{y}(\mathbf{s})$ are the observed variables and underlying processes, respectively. We also denote the vector-valued mean function and error process as $\boldsymbol{\mu}(\mathbf{s})$ and $\boldsymbol{\epsilon}(\mathbf{s})$, respectively. For example, consider the following model

$$\mathbf{z}(\mathbf{s}) = \boldsymbol{\mu}(\mathbf{s}) + \mathbf{y}(\mathbf{s}) + \boldsymbol{\epsilon}(\mathbf{s}), \quad (9)$$

where $\boldsymbol{\mu}(\mathbf{s}) = \boldsymbol{\mu}$ and $\boldsymbol{\epsilon}(\mathbf{s}) \stackrel{iid}{\sim} \mathcal{N}(\mathbf{0}, \text{diag}(\sigma_1^2, \dots, \sigma_N^2))$. Models of this form are common in many multivariate spatial applications (e.g., see Banerjee et al., 2004; Cressie and Wikle, 2011) so the difference in models then becomes how one parameterizes the dependence structure of $\mathbf{y}(\mathbf{s})$. Many researchers use full-rank cross-covariance models to estimate the joint covariance matrix (e.g., see the review in Genton and Kleiber, 2015). Alternatively, one can use a low-rank estimate of the covariance matrix using a basis function model, which was the primary idea in univariate CAGE (Bradley et al., 2017). We extend this to multivariate processes and call it the multivariate Obled-Creutin (MVOC) approach as explained below.

We consider the following modeling assumptions in our example to demonstrate the MVOC approach. For the j -th univariate process, we select a set of prescribed orthonormal basis functions: $\{\phi_{jk}(\mathbf{s}) : \mathcal{S} \rightarrow \mathbb{R}\}_{k=1}^{\tilde{M}_j}$. Using these basis functions, we consider the following modeling assumption

$$Y_j(\mathbf{s}) = \sum_{k=1}^{\tilde{M}_j} \phi_{jk}(\mathbf{s}) \nu_{jk}. \quad (10)$$

We denote the orthonormal basis matrix $\Phi_j \in \mathbb{R}^{n \times \widetilde{M}_j}$ as the $n \times \widetilde{M}_j$ matrix with k, ℓ -th element as $\phi_{j\ell}(\mathbf{s}_k)$. These are the univariate Obled-Creutin (OC) bases that were used in the derivation of the univariate CAGE criterion in Bradley et al. (2017). We then define the joint OC basis as the block matrix Φ with i, j -th block as Φ_j for $i = j$, $\mathbf{0}$ when $i \neq j$. Next, denote \mathbf{z}^{vec} as the $Nn \times 1$ vector version of the $n \times N$ matrix of the observations $\mathbf{z}(\mathbf{s})$. Define \mathbf{y}^{vec} , $\boldsymbol{\nu}^{\text{vec}}$, and $\boldsymbol{\epsilon}^{\text{vec}}$ similarly. Then, in matrix form, the modeling assumptions (9) and (10) are equivalent to

$$\mathbf{z}^{\text{vec}} = \boldsymbol{\mu}^{\text{vec}} + \mathbf{y}^{\text{vec}} + \boldsymbol{\epsilon}^{\text{vec}},$$

where $\mathbf{y}^{\text{vec}} = \Phi \boldsymbol{\nu}^{\text{vec}}$. Now, within a Bayesian inferential framework, we use the following prior assumptions

$$\begin{aligned} \mu_j &\propto 1, \\ \epsilon_j(\mathbf{s}) &\stackrel{iid}{\sim} \mathcal{N}(0, \sigma_j^2), \\ \boldsymbol{\nu}_j = (\nu_{j1}, \dots, \nu_{jM_j}) &\sim \mathcal{N}(0, g\sigma_j^2 (\Phi_j^\top \Phi_j)^{-1}), \\ \sigma_j^2 &\sim \text{Inverse Gamma}(a_j^\sigma, b_j^\sigma), \end{aligned}$$

where in our examples, we used $a_j^\sigma = b_j^\sigma = 0$, which corresponds to the Jeffrey's prior $\sigma_j^2 \propto \frac{1}{\sigma_j^2}$. The above formulation is known as Zellner's g-prior (Zellner, 1986), which is often used in penalized regression and variable selection (e.g., see a review in Agliari and Parisetti, 1988). After experimenting with many possible choices, we use $g = n$ in our examples, which is interpreted as the prior having the equivalent weight of one observation. Note that more complicated models and prior choices can be used here, and our only goal is to estimate the joint covariance matrix \mathbf{C} . The posterior samples are obtained via a block Gibbs sampler, where each parameter is sampled in sequence from its full conditional distribution (refer to Appendix C for the details).

To estimate the KLE from the MVOC basis model, we use the following procedure. From the posterior chain of the hyperparameters, draw a set of expansion coefficients as $\widehat{\boldsymbol{\nu}}_1^{\text{vec}}, \widehat{\boldsymbol{\nu}}_2^{\text{vec}}, \dots, \widehat{\boldsymbol{\nu}}_T^{\text{vec}} \sim$

$\pi(\boldsymbol{\nu}^{\text{vec}}|\mathbf{Z})$. Estimate the posterior covariance matrix of $\boldsymbol{\nu}^{\text{vec}}$ as $\widehat{\boldsymbol{\Sigma}}$ from these samples, and perform the eigendecomposition as $\widehat{\boldsymbol{\Sigma}} = \mathbf{E}\boldsymbol{\Lambda}\mathbf{E}^\top$. Similar to Section 2.3, denote the k -th column of \mathbf{E} as the vector \mathbf{e}_k and express it in the following block-vector form: $\mathbf{e}_k^\top = (\mathbf{e}_k^1, \dots, \mathbf{e}_k^N)$. Then, the j -th element of the k -th eigenfunction and the expansion coefficients are given by

$$\begin{aligned} [\boldsymbol{\psi}_k(\mathbf{s})]_j &= (\phi_{j1}(\mathbf{s}), \dots, \phi_{jM_j}(\mathbf{s}))^\top \mathbf{e}_k^j \\ \alpha_k &= \sum_{j=1}^N (\nu_{j1}, \dots, \nu_{jM_j})^\top \mathbf{e}_k^j. \end{aligned} \tag{11}$$

The proof of the correctness of this expression can be found in Appendix D.

Remark 3.1. One may wish to utilize distance-based basis functions in the first step since the choices of the orthonormal basis families can be limited. In spatial statistics, distance-based basis functions (such as radial basis, Bisquare basis, Wendland basis, Matérn basis, etc.) are intuitive and used more than polynomial or Fourier bases for building models. We denote such basis functions as “generating basis functions” or GBFs. The use of such bases requires an additional decorrelation step to get orthonormal basis functions. Let $\{\theta_{jk}\}_{k=1}^{\widetilde{M}_j}$ be the distance-based basis functions, and define the matrix \mathbf{W}_j with k, ℓ -th element given by $w_{k\ell}^j = \int_{\mathbf{s}} \theta_{jk}(\mathbf{s})\theta_{j\ell}(\mathbf{s}) d\mathbf{s}$. Assuming positive-definiteness of \mathbf{W}_j , \mathbf{Q}_j is defined as the inverse Cholesky decomposition of \mathbf{W}_j , i.e., $\mathbf{W}_j^{-1} = \mathbf{Q}_j\mathbf{Q}_j^\top$.

We then decorrelate the GBFs to get orthonormal basis functions

$$(\phi_{j1}(\mathbf{s}), \dots, \phi_{j\widetilde{M}_j}(\mathbf{s})) = (\phi_{j1}(\mathbf{s}), \dots, \phi_{j\widetilde{M}_j}(\mathbf{s}))^\top \mathbf{Q}_j.$$

Remark 3.2. Note that M_j is always less than or equal to \widetilde{M}_j , and one can set $M_j = \widetilde{M}_j$. Alternatively, one can discard the trailing eigenvalues of \mathbf{U}_j if their values are too small and indistinguishable from each other (e.g., Hastie et al., 2009)

3.3 Alternative Modeling and MKLE Computation

We also demonstrate a few examples using alternative covariance modeling techniques. In particular, for cross-covariance models, we employ the linear model for co-regionalization (LMC) (Journal

and Huijbregts, 1978; Goulard and Voltz, 1992) to estimate the full covariance matrix of \mathbf{z}^{vec} . Interested readers can see Wackernagel et al. (1989) for a survey on co-regionalization. Specifically, we use the co-kriging procedure from the R package `gstat` (Gräler et al., 2016; Rossiter, 2007). For a bivariate process, the LMC first models one of the spatial processes (say $Z_1(\mathbf{s})$) using the traditional geospatial model (Cressie and Wikle, 2011). Then, the second spatial process is built as a conditional model using $Z_1(\mathbf{s})$, i.e., we estimate the distribution of $\pi[Z_2(\mathbf{s})|Z_1(\mathbf{s})]$. We use this approach to estimate the underlying parameters of the covariance matrix (cf. Appendix E for an example).

We consider another example of empirical MKLE with the assumption of repeated data. When sufficient multiple replications of the multivariate variables are available, i.e., more samples than the number of parameters are available, one can compute the empirical covariance matrix of the data as

$$\widehat{\mathbf{C}}_{ij}(\mathbf{s}, \mathbf{r}) = \frac{1}{\tilde{n}} \sum_{k=1}^{\tilde{n}} [Z_{i,k}(\mathbf{s}) - \bar{Z}_i(\mathbf{s})][Z_{j,k}(\mathbf{r}) - \bar{Z}_j(\mathbf{r})]^\top, \quad (12)$$

where $Z_{j,k}$ is the k -th replication of the j -th process and $\bar{Z}_j(\mathbf{s}) = \frac{1}{\tilde{n}} \sum_{k=1}^{\tilde{n}} Z_{j,k}(\mathbf{s})$ (cf. Section 4.1 for an example).

If we first estimate the form covariance functions $\widehat{\mathbf{C}}_{jk}$, we need to compute the MKLE from them. We use the Galerkin approach (Ghanem and Spanos, 1991) here, which is a similar routine as used in the MVOC basis construction. To compute the KLE for the j -th univariate process, we start with a set of orthonormal basis functions $\{\phi_{jk}(\mathbf{s})\}_{k=1}^{\tilde{M}_j}$. Such families of basis functions include Fourier, Haar, spline, polynomial basis functions, and many others. Given the estimate $\widehat{\mathbf{C}}_{jj}(\mathbf{s}, \mathbf{r})$, one can compute the matrix \mathbf{U}_j with elements $U_{k\ell}^j$ as

$$U_{k\ell}^j = \int_{\mathbf{s}} \int_{\mathbf{r}} \widehat{\mathbf{C}}_{jj}(\mathbf{s}, \mathbf{r}) \phi_{jk}(\mathbf{s}) \phi_{j\ell}(\mathbf{r}) d\mathbf{s} d\mathbf{r}.$$

Assuming the positive definiteness of \mathbf{U}_j , we can perform an eigendecomposition on \mathbf{U}_j to get eigenvalues $\lambda_{j1} \geq \dots \geq \lambda_{jM_j}$ and eigenvectors $\mathbf{f}_{j1}, \dots, \mathbf{f}_{jM_j}$. Then, the k -th eigenfunction of $\widehat{\mathbf{C}}_{jj}$ is

given by

$$\psi_{jk}(\mathbf{s}) = (\phi_{j1}(\mathbf{s}), \dots, \phi_{j\tilde{M}_j}(\mathbf{s}))^\top \mathbf{f}_{jk}.$$

Proof of the correctness of this derivation is provided in Appendix F.

Remark 3.3. Note that if the number of replications are less than the rank of the covariance matrix, one can use a similar technique as in the MVOC approach to approximate the first few eigenpairs. In that case, using the OC basis, we assume the following basis expansion model

$$Z_{j,k}(\mathbf{s}) = \mu_j + \sum_{i=1}^{\tilde{M}_j} \phi_{ji}(\mathbf{s}) \nu_{ji}^k + \epsilon_j(\mathbf{s}),$$

where, like before, $Z_{j,k}(\mathbf{s})$ is the k -th replication of the j -th process, and ν_{ji}^k is the i -th basis expansion for the k -th replication of the j -th process. Then, we can compute the covariance matrix \mathbf{K}_{jm} between the expansion coefficients with its k, ℓ -th element given by $\frac{1}{n} \sum_{i=1}^{\tilde{n}} (\nu_{jk}^i - \bar{\nu}_{jk})(\nu_{m\ell}^i - \bar{\nu}_{m\ell})^\top$, where $\bar{\nu}_{jk} = \frac{1}{n} \sum_{i=1}^{\tilde{n}} \nu_{jk}^i$. Following a similar procedure as in the MVOC basis, we decorrelate the block matrix \mathbf{K} with blocks \mathbf{K}_{jk} to find the multivariate eigenfunctions and eigenvalues.

3.4 Spatial Regionalization

Given the multivariate eigenfunctions and eigenvalues from Sections 3.2 or 3.3, we compute the regionalization in this section. Here, we apply a similar two-stage regionalization algorithm as in univariate CAGE (Bradley et al., 2017). In the first stage, we employ a spatial clustering algorithm (e.g., spatial k -means, HGC, MST) that finds a set of candidate supports. In the second stage, the MVCAGE (or DMVCAGE) statistic is computed over these supports and the minimum statistic is retained. Bradley et al. (2017) argues that in the context of the univariate CAGE, this methodology is more computationally efficient than a global search of minimum CAGE since the total number of possible choices is of combinatorial order in the number of partitions. This is also true for

MVCAGE. However, as mentioned in Section 3.1, here we used the HGC with Ward clustering on the space of the KLE, which generated spatially contiguous partitions. An additional benefit of using HGC is that, since we need to compare MVCAGE statistic for different choices of number of clusters, we can implement parallel processing after computing the linkages (or dendrogram) once.

Unlike the univariate CAGE, where the authors used two hyperparameters for the maximum and minimum number of areal units considered, we use one user-defined stopping criterion in our study to find an optimal choice of number of clusters. For a given number of clusters, we compute the MVCAGE statistic and keep proceeding until the relative change in MVCAGE for two consecutive clusters becomes very close. Although this choice of the stopping parameter is user-defined, one can use similar ideas as the elbow or Silhouette plot for k -means clustering to have a data-driven guess. The complete algorithm for regionalization with MVCAGE is given by Algorithm 1.

Algorithm 1 Spatial Regionalization with MVCAGE

- 1: **Input** Multivariate data $\mathbf{z}(\mathbf{s}) = (Z_1(\mathbf{s}), \dots, Z_N(\mathbf{s}))^\top$ at locations $\mathbf{S} = \{\mathbf{s}_1, \dots, \mathbf{s}_n\}$. Model specification \mathbb{M} . Stopping parameter ϵ for the number of regions under consideration.
- 2: Fit the model \mathbb{M} to estimate the underlying processes $\mathbf{y}(\mathbf{s})$ and their covariance functions \widehat{C}_{ij} (Section 3.2).
- 3: Use the Galerkin method to compute the univariate KLEs of \widehat{C}_{ij} (Section 3.3).
- 4: Compute the multivariate KLE for the fitted multivariate covariance function \mathbb{C} (Section 2.3).
- 5: $j = 1$.
- 6: **while** true **do**
 - a: Use HGC on $\mathbf{y}(\mathbf{s}_1), \dots, \mathbf{y}(\mathbf{s}_n)$ to find j number of candidate supports.
 - b: Compute the $MC_j = MVCAGE$ for these candidate supports.
 - c: **if** $\frac{MC_{j-1} - MC_j}{MC_{j-1}} < \epsilon$ **break**.
 - d: $j = j + 1$.

7: *end while*

8: Return the clustering output of HGC.

4 Simulation and Applications

We illustrate our methodology in this section using simulated data and data from demographic application. We use a simulated dataset with repeated observations in Section 4.1 and demonstrate the MVCAGE regionalization using empirical KLE. In Section 4.2, using American Community Survey (ACS) and hospital quality data, we show the application with MVOC basis functions and Bayesian computation of the MKLE. Additionally, in Appendix E, we demonstrate the covariance estimation using LMC and apply it to an ocean color dataset.

4.1 Simulation: Empirical KLE-based MVCAGE for Functional data

We consider one-dimensional (in space) bivariate simulated data from a full bivariate Matérn process (Guttorp and Gneiting, 2006; Gneiting et al., 2010) over the one-dimensional region $[0, 1]$ with the covariance functions \mathbb{C} that take the following form:

$$\mathcal{M}(\mathbf{s}, \mathbf{r}; \nu, a) = \frac{2^{1-\nu}}{\Gamma(\nu)} (a\|\mathbf{s} - \mathbf{r}\|)^\nu \mathbb{K}_\nu(a\|\mathbf{s} - \mathbf{r}\|),$$

$$\mathbb{C}_{ii}(\mathbf{s}, \mathbf{r}) = \sigma_i^2 \mathcal{M}(\mathbf{s}, \mathbf{r}; \nu_{ii}, a_{ii}),$$

$$\mathbb{C}_{ij}(\mathbf{s}, \mathbf{r}) = \rho \sigma_i \sigma_j \mathcal{M}(\mathbf{s}, \mathbf{r}; \nu_{ij}, a_{ij}).$$

We use the following parameter set for the simulation: $a_1 = 10$, $a_2 = 15$, $a_{12} = 1.2 \max(a_1, a_2)$, $\nu_1 = 0.4$, $\nu_2 = 0.5$, $\nu_{12} = 0.5(\nu_1 + \nu_2)$. We randomly select 1000 locations over $[0, 1]$ and generate $r = 4000$ replications of the bivariate spatial data.

Since we have multiple replications here, we use the low-rank empirical MKLE (Equation 12) in this example. We compute the MKLE of the joint covariance kernel using $K = 50$ sets of Fourier basis functions, i.e., $\phi_{j1}(s) = 1$, $\phi_{jk}(s) = (\sin(2\pi \frac{k-1}{50} s), \cos(2\pi \frac{k-1}{50} s))$ for $k = 1, \dots, 50$. This choice

leads to a total of 101 basis functions. We use these basis functions to estimate the expansion coefficient and then decorrelate them to compute the MKLE of the covariance kernels. Based on that, we compute the MCAGE loss function.

We next use 5,000 pseudo-points over the domain for the clustering. We consider 10^{-4} as the stopping criterion. The final selection of the number of clusters is 97. Figure 1 shows a realization of the simulated data (i.e., $Z_1(s)$ and $Z_2(s)$) and demonstrates its aggregated version (i.e., $\hat{z}(s)$) after applying MVCAGE. Figure 2 shows the quantity of MVCAGE using (6).

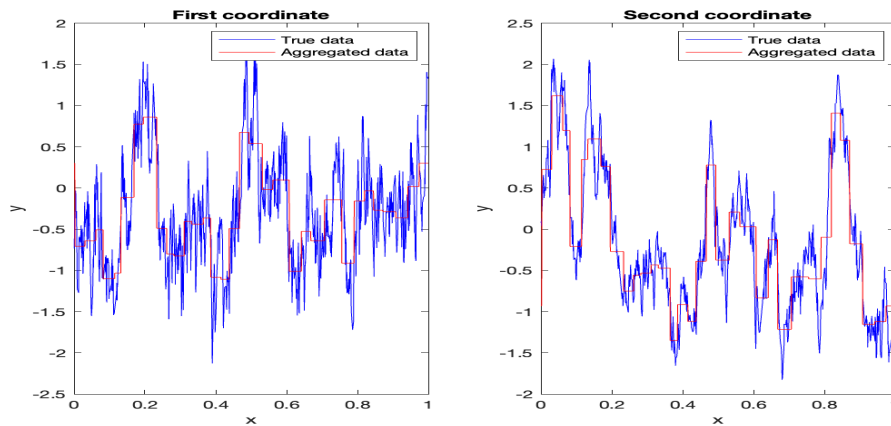


Figure 1: **Regionalization with MVCAGE for data from a one-dimensional bivariate Matérn process:** We applied MVCAGE to aggregate sample data from bivariate Matérn Process. The blue lines correspond to the simulated data over 1000 locations between $[0,1]$. The left panel shows the original (in blue) and aggregated data (in red) for the first process. The right panel shows the same for the second process.

4.2 U.S. County-level Regionalization

We apply our methodology to regionalize the counties of the United States using a bivariate dataset consisting of log median income and hospital quality ratings. We considered the data from 3106 counties in 2015 that had no missing data. The log median income data consists of public-use

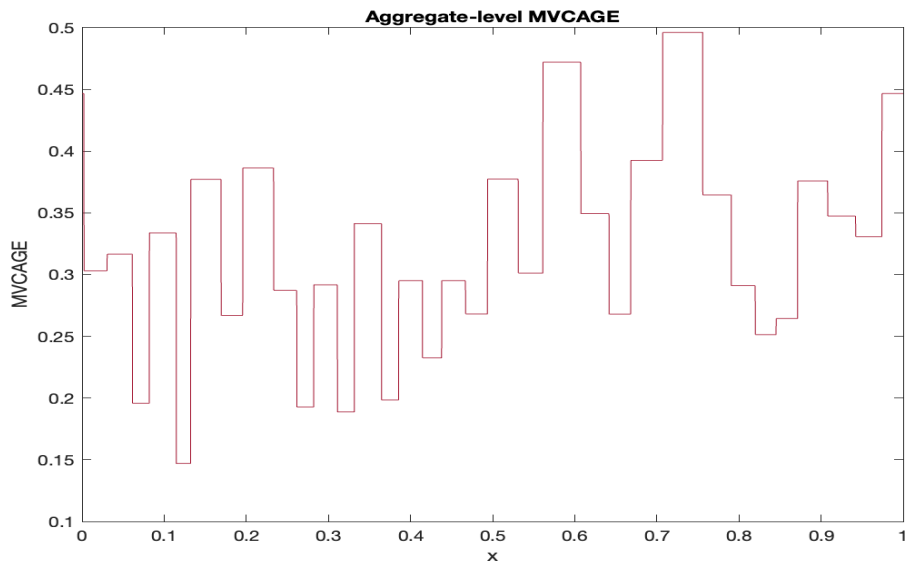


Figure 2: **Value of MVCAGE over the areal units:** Plot of the MVCAGE statistic over the areal regions for the optimal choice of regionalization. The larger the MVCAGE value, the greater is the potential for the ecological fallacy to occur during inference.

county-level 5-year period estimates from the American Community Survey¹ and can be easily accessed using R package `tidycensus`. The hospital quality ratings are obtained through the Dartmouth Atlas Study², which is a research initiative focused on healthcare analysis across the United States. We use the adjusted ratings data for the U.S. counties based on the primary care access and quality measures available at the respective hospitals.

We used a MVOC basis approach here. To construct the spatial OC basis, we started with 300 Gaussian basis functions as the GBF. We computed 300 OC basis functions from these GBFs following the ideas in Remark 3.1. For the regionalization algorithm, we used a stopping criterion of 0.01 and the final number of areal units is 96. The final constructed areal data is shown in Figure 3. The regionalization is shown in Figure 4. The MVCAGE regionalization shows 97 broad contiguous spatial regions in both variables. This represents a substantial dimension reduction

¹<https://www.census.gov/programs-surveys/acs>

²<https://www.dartmouthatlas.org/>

from the county data.

These two particular variables allow us to assess the discrepancy in areas in need (i.e., log income can be used as a proxy for an area in need) and the quality of the hospitals in that area. In the bottom-left panel of Figure 3, we see that relatively lower log incomes tend to arise in the southeast, southwest, and northwest US, with central areas and northeast regions of the US having slightly larger log incomes. In contrast, in the bottom-right panel, the hospital quality metrics tend to be larger only in eastern US. This suggests that several regions on the West Coast and central US have an indirect relationship between log income and hospital quality. Regionalization is particularly useful for coming to these conclusions as the fine-scale features of the country-level observations obfuscate these trends.

We note that this analysis is meant as an illustration and did not directly consider the sampling error variance in the ACS survey data. In principle, such uncertainties could be included in the data model of the hierarchical framework, possibly leading to different regionalizations. The consideration of measurement and sampling error on regionalization is an interesting topic, but is beyond the scope of the current work.

5 Discussion

In this manuscript, we propose a methodology for the multivariate regionalization of spatial data. The core of our methodology is the multivariate KLE of the underlying spatial processes. The KLE is the \mathcal{L}_2 -optimal linear expansion of any spatial process. It also satisfies the bi-orthogonality property by using uncorrelated expansion coefficients and orthonormal eigenfunctions. In the multivariate domain, the expression of the eigenfunctions is complicated due to the cross-covariance structures between the different spatial processes. Here we demonstrate how to build multivariate eigenfunctions starting from the univariate process-specific and cross-covariance matrices. More-

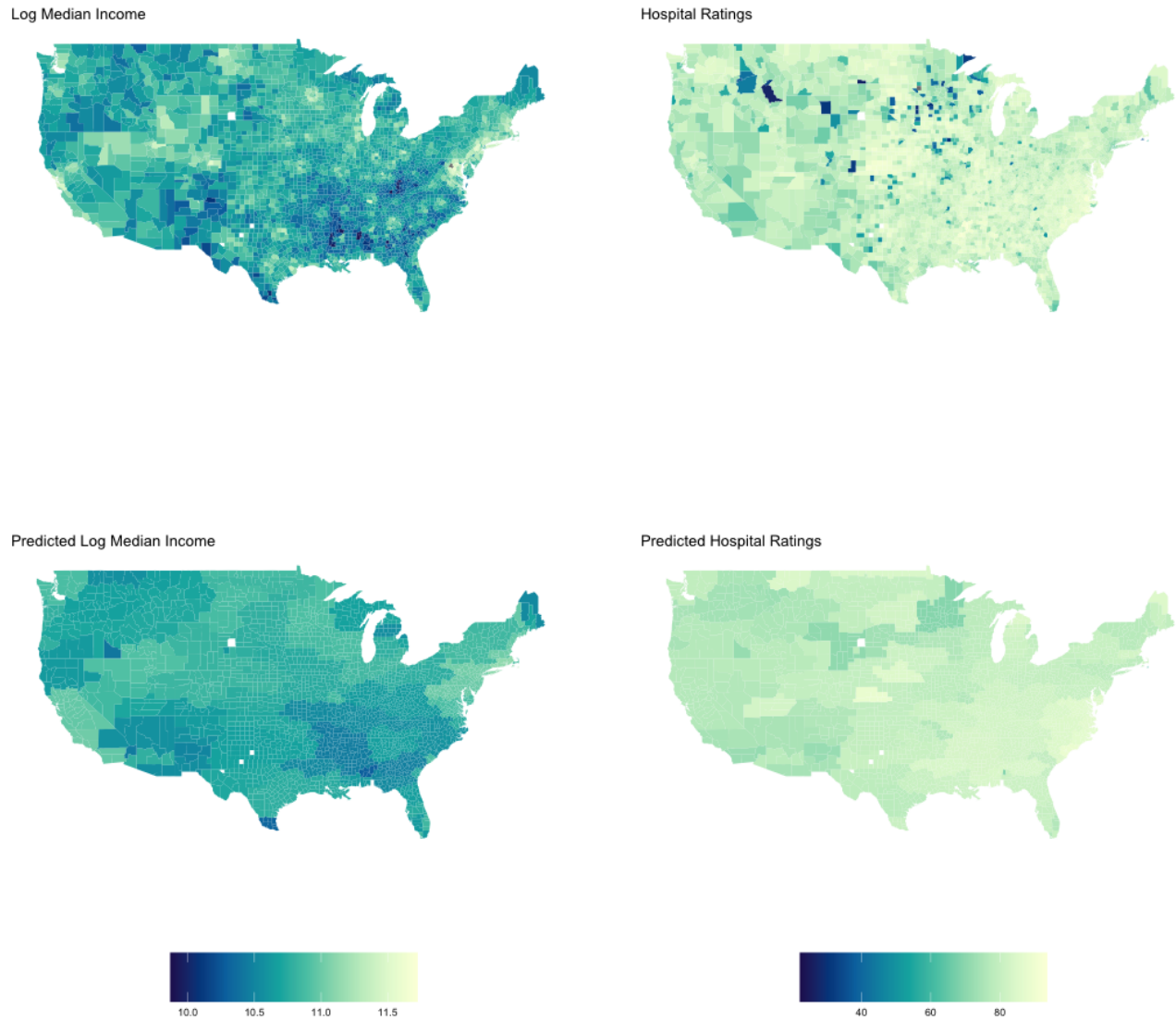


Figure 3: **Regionalization of Bivariate log median income and Hospital Quality Data over US counties with MVCAGE:** We applied our methodology to aggregate the counties over the U.S. using the ACS 5-year period estimate of log median income and the Dartmouth Atlas Study hospital quality ratings from 2015. The left column shows the county-level (top) and the area-level (bottom) aggregation of the log median income data. The right column demonstrates the same for the quality ratings.

Joint Regionalization of Log Median Income and Hospital Ratings

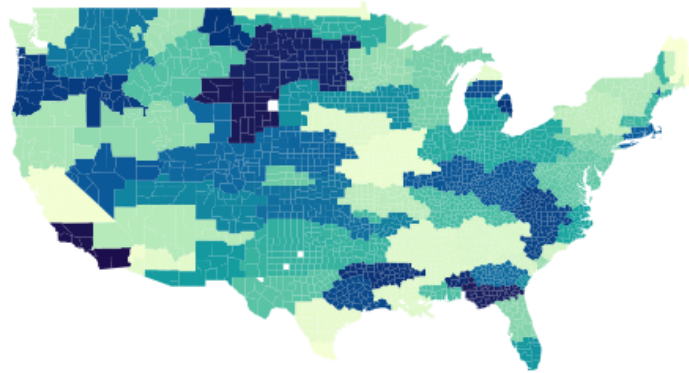


Figure 4: **Regions using MVCAGE for Bivariate Regionalization of U.S. counties with MVCAGE:** We show the regions from the bivariate regionalization of the U.S. counties the ACS 5-year period estimate of log median income and the Dartmouth Atlas Study hospital quality ratings from 2015.

over, we also show the application of the multivariate Obled-Cruetin basis functions to propose an alternative Bayesian computation of the multivariate KLE. All the procedures are similar in the following sense. We start with any set of orthonormal basis functions and assume that the multivariate eigenfunctions lie on the span of these basis functions. We then compute the expansion coefficients and their joint covariance matrix. Decorrelating this matrix gives us the necessary eigenpairs.

The principal goal of applying the MKLE-based loss function is to minimize the ecological fallacy in a spatial COS procedure. Spatial COS changes the resolution of the spatial supports. It often comes with Simpson's paradox-like behavior in that the original and the aggregated data may

demonstrate two different spatial patterns. Although researchers have studied the ecological fallacy extensively, there has been little development to quantify the amount of the ecological fallacy and minimize this when performing spatial aggregation. Here, we use the logic of the univariate CAGE method by Bradley et al. (2017) and extend it to the multivariate domain. We demonstrate how to compute the area-level eigenfunctions, defined as the continuous average of the corresponding point-level eigenfunctions over any given areal region. We then use any loss function (such as \mathcal{L}_1 , \mathcal{L}_2) to compute the distance between the point-level and areal-level eigenfunctions, with eigenvalues used as weights. The MVCAGE loss over any areal region is the continuous average of this loss function. We provide a discussion and proposition on why minimizing the MVCAGE loss leads to a lower value of the ecological fallacy in spatial aggregation.

In practice, we need to use a discrete approximation of the MVCAGE statistic using a set of gridded points and Monte Carlo approximations. If the original data is in an areal format, we can approximate the eigenfunctions within each areal region by using the Monte Carlo approximation. If the data is in a continuous point format, we can use regular grid areas as the original areal units and proceed similarly. Our goal is to find the regionalization with the minimum MVCAGE. As discussed by Bradley et al. (2017), finding the global minimum value of MVCAGE for all possible combinations of spatial units is computationally expensive. MVCAGE instead uses an alternate two-stage regionalization algorithm. The first stage of the regionalization algorithm uses the estimated values of the underlying spatial processes and applies any spatial clustering method to propose a set of candidate supports. For this, we specify lower and upper bounds on the number of possible regions or clusters. In the second stage, we compute MVCAGE for all these supports and retain the one with the minimum MVCAGE. This way, we find the particular regionalization with the minimum value of MVCAGE. We illustrated the application of the MVCAGE algorithm using a simulated data example and through an application to demographic and ocean color datasets.

There are several opportunities for future research based on the ideas proposed here. For

example, extension of the MKLE to the spatio-temporal setting would provide a useful tool for investigating aggregation in both space and time. Another useful extension would be to consider different penalization on the number of regions. Lastly, an interesting direction of research would be to study the behavior of the global vs. local eigenfunctions of the corresponding MKLEs.

Acknowledgments

This article is released to inform interested parties of ongoing research and to encourage discussion. The views expressed on statistical issues are those of the authors and not those of the NSF or U.S. Census Bureau. This research was partially supported by the U.S. National Science Foundation (NSF) under NSF grants SES-1853096, NCSE-2215168, DMS-2310756.

References

- Agliari, A. and Parisetti, C. C. (1988). A-g reference informative prior: A note on zellner’s g-prior. *Journal of the Royal Statistical Society: Series D (The Statistician)*, 37(3):271–275.
- Alexandrov, T. and Kobarg, J. H. (2011). Efficient spatial segmentation of large imaging mass spectrometry datasets with spatially aware clustering. *Bioinformatics*, 27(13):i230–i238.
- Anselin, L. (1988). *Spatial Econometrics: Methods and Models*. Springer-Verlag.
- Aronszajn, N. (1950). Theory of reproducing kernels. *Transactions of the American Mathematical Society*, 68(3):337–404.
- Assunção, R. M., Neves, M. C., Câmara, G., and da Costa Freitas, C. (2006). Efficient regionalization techniques for socio-economic geographical units using minimum spanning trees. *International Journal of Geographical Information Science*, 20(7):797–811.

- Bacao, F., Lobo, V., and Painho, M. (2005). Applying genetic algorithms to zone design. *Soft Computing*, 9:341–348.
- Bailey, T. C. and Gatrell, A. C. (1995). *Interactive Spatial Data Analysis*. Longman Scientific & Technical.
- Banerjee, S., Carlin, B. P., and Gelfand, A. E. (2004). *Hierarchical Modeling and Analysis for Spatial Data*. CRC press.
- Bezdek, J. C. (1981). Pattern recognition with fuzzy objective function algorithms. *Plenum Press*, 1.
- Borcard, D., Legendre, P., and Drapeau, P. (1992). Partialling out the spatial component of ecological variation. *Ecology*, 73(3):1045–1055.
- Bradley, J. R., Wikle, C. K., and Holan, S. H. (2017). Regionalization of multiscale spatial processes by using a criterion for spatial aggregation error. *Journal of the Royal Statistical Society: Series B (Statistical Methodology)*, 79(3):815–832.
- Chavent, M., Kuentz-Simonet, V., Labenne, A., and Saracco, J. (2018). Clustgeo: an R package for hierarchical clustering with spatial constraints. *Computational Statistics*, 33(4):1799–1822.
- Chen, Z., Fan, J., and Wang, K. (2023). Multivariate Gaussian processes: definitions, examples and applications. *METRON*, pages 1–11.
- Cho, H., Venturi, D., and Karniadakis, G. (2013). Karhunen-Loève expansion for multi-correlated stochastic processes. *Probabilistic Engineering Mechanics*, 34:157–167.
- Cressie, N. and Wikle, C. K. (2011). *Statistics for Spatio-temporal Data*. John Wiley & Sons.
- Cressie, N. and Zammit-Mangion, A. (2016). Multivariate spatial covariance models: a conditional approach. *Biometrika*, 103(4):915–935.

- Daw, R., Simpson, M., Wikle, C. K., Holan, S. H., and Bradley, J. R. (2022). An overview of univariate and multivariate Karhunen-Loève expansions in statistics. *Journal of the Indian Society for Probability and Statistics*, 23(2):285–326.
- Daw, R. and Wikle, C. K. (2022). Supervised spatial regionalization using the Karhunen-Loève expansion and minimum spanning trees. *Journal of Data Science*, 20(4):566–584.
- Duque, J. C., Anselin, L., and Rey, S. J. (2012). The max-p-regions problem. *Journal of Regional Science*, 52(3):397–419.
- Duque, J. C., Ramos, R., and Suriñach, J. (2007). Supervised regionalization methods: a survey. *International Regional Science Review*, 30(3):195–220.
- Elliot, P., Wakefield, J. C., Best, N. G., Briggs, D. J., et al. (2000). *Spatial Epidemiology: Methods and Applications*. Oxford University Press.
- Fotheringham, A. S., Brunson, C., and Charlton, M. (2000). Geographically weighted regression: the analysis of spatially varying relationships. *John Wiley & Sons*.
- Gelfand, A. E. (2021). Multivariate spatial process models. *Handbook of Regional Science*, pages 1985–2016.
- Genton, M. G. and Kleiber, W. (2015). Cross-covariance functions for multivariate geostatistics. *Statistical Science*, 30(2):147 – 163.
- Ghanem, R. and Spanos, P. D. (1991). Stochastic finite elements: a spectral approach. *Springer Science & Business Media*.
- Gneiting, T., Kleiber, W., and Schlather, M. (2010). Matérn cross-covariance functions for multivariate random fields. *Journal of the American Statistical Association*, 105(491):1167–1177.

- Gotway, C. A. and Young, L. J. (2002). Combining incompatible spatial data. *Journal of the American Statistical Association*, 97(458):632–648.
- Goulard, M. and Voltz, M. (1992). Linear coregionalization model: tools for estimation and choice of cross-variogram matrix. *Mathematical Geology*, 24:269–286.
- Gräler, B., Pebesma, E., and Heuvelink, G. (2016). Spatio-temporal interpolation using gstat. *The R Journal*, 8:204–218.
- Guha, S., Rastogi, R., and Shim, K. (1998). CURE: An efficient clustering algorithm for large databases. In *ACM SIGMOD Conference*. ACM.
- Guttorp, P. and Gneiting, T. (2006). Studies in the history of probability and statistics XLIX on the matérn correlation family. *Biometrika*, 93(4):989–995.
- Haidvogel, D. B., Arango, H. G., Budgell, W. P., Cornuelle, B. D., Curchitser, E., Di Lorenzo, E., Fennel, K., Geyer, W. R., Hermann, A. J., Lanerolle, L., Levin, J., McWilliams, J. C., Miller, A. J., Moore, A. M., Powell, T. M., Shchepetkin, A. F., Sherwood, C. R., Signell, R. P., Warner, J. C., and Wilkin, J. (2010). Ocean forecasting in terrain-following coordinates: formulation and skill assessment of the regional ocean modeling system. *Monthly Weather Review*, 138(2):619–646.
- Happ, C. and Greven, S. (2018). Multivariate functional principal component analysis for data observed on different (dimensional) domains. *Journal of the American Statistical Association*, 113(522):649–659.
- Hastie, T., Tibshirani, R., Friedman, J. H., and Friedman, J. H. (2009). *The elements of statistical learning: data mining, inference, and prediction*, volume 2. Springer.

- He, X., Tao, Y., Wang, Q., and Lin, H. (2019). Multivariate spatial data visualization: a survey. *Journal of visualization*, 22:897–912.
- Journel, A. G. and Huijbregts, C. J. (1978). Mining geostatistics. *Journal of International Association for Mathematical Geology*, 10(4):395–424.
- Karhunen, K. (1947). Zur spektraltheorie stochastischer prozesse. *Annales Academiae Scientiarum Fennicae*, 37:1–79.
- Lawson, A. B. and Clark, A. (2002). Spatial mixture relative risk models applied to disease mapping. *Statistics in medicine*, 21(3):359–370.
- Leeds, W. B., Wikle, C. K., and Fiechter, J. (2014). Emulator-assisted reduced-rank ecological data assimilation for nonlinear multivariate dynamical spatio-temporal processes. *Statistical Methodology*, 17:126–138.
- Loève, M. (1945). *Probability Theory*, volume 1. Van Nostrand Princeton.
- MacQueen, J. (1967). Some methods for classification and analysis of multivariate observations. In LeCam, L. M. and Neyman, J., editors, *Proceedings of the Fifth Berkeley Symposium on Mathematical Statistics and Probability*, volume 1, pages 281–297. University of California Press.
- Mennis, J. (2002). Generating surface models of population using dasymetric mapping. *The Professional Geographer*, 54(1):31–42.
- Openshaw, S. (1979). A million or so correlated coefficients: three experiment on the modifiable areal unit problem. *Statistical applications in the spatial sciences*.
- Openshaw, S. (1984). The modifiable areal unit problem. *Concepts and Techniques in Modern Geography*, 38:41–57.

- Peña-Angulo, D., Vicente-Serrano, S. M., Domínguez-Castro, F., Lorenzo-Lacruz, J., Murphy, C., Hannaford, J., Allan, R. P., Trambly, Y., Reig-Gracia, F., and El Kenawy, A. (2022). The complex and spatially diverse patterns of hydrological droughts across Europe. *Water Resources Research*, 58(4):e2022WR031976.
- Quinlan, J. R. (1986). Induction of decision trees. *Machine Learning*, 1:81–106.
- Rasmussen, C. E. and Williams, C. K. (2006). *Gaussian processes for machine learning*. MIT press.
- Robinson, W. S. (2009). Ecological correlations and the behavior of individuals. *International Journal of Epidemiology*, 38(2):337–341.
- Rossiter, D. (2007). Co-kriging with the gstat package of the R environment for statistical computing. Web: <http://www.itc.nl/rossiter/teach/R/Rck.pdf>.
- Sneath, P. H. A. and Sokal, R. R. (1962). Numerical taxonomy. *Nature*, 193(4812):855–860.
- Tatem, A. J., Lewis, H. G., Atkinson, P. M., and Nixon, M. S. (2003). Increasing the spatial resolution of agricultural land cover maps using a hopfield neural network. *International Journal of Geographical Information Science*, 17(7):647–672.
- Ver Hoef, J. M. and Barry, R. P. (1998). Constructing and fitting models for cokriging and multivariable spatial prediction. *Journal of Statistical Planning and Inference*, 69(2):275–294.
- Ver Hoef, J. M. and Cressie, N. (1993). Multivariable spatial prediction. *Mathematical Geology*, 25:219–240.
- Wackernagel, H., Petitgas, P., and Touffait, Y. (1989). Overview of methods for coregionalization analysis. In *Geostatistics: Proceedings of the Third International Geostatistics Congress September 5–9, 1988, Avignon, France*, pages 409–420. Springer.

- Ward Jr, J. H. (1963). Hierarchical grouping to optimize an objective function. *Journal of the American Statistical Association*, 58(301):236–244.
- Wikle, C. K. and Berliner, L. M. (2005). Combining information across spatial scales. *Technometrics*, 47(1):80–91.
- Wikle, C. K., Milliff, R. F., Herbei, R., and Leeds, W. B. (2013). Modern statistical methods in oceanography: a hierarchical perspective. *Statistical Science*, 28:466–486.
- Zellner, A. (1986). An introduction to Bayesian inference in Econometrics. *John Wiley & Sons*.
- Zhou, S. and Bradley, J. R. (2023). Bayesian hierarchical modeling for bivariate multiscale spatial data with application to blood test monitoring. *arXiv preprint arXiv:2310.13580*.

Supplemental Material for A Criterion for Multivariate Regionalization of Spatial Data

Appendix A MKLE Construction from Univariate KLEs

Denote $\tilde{\boldsymbol{\alpha}}$ as the collection of all the process-specific expansion coefficients, i.e., $\tilde{\boldsymbol{\alpha}} = (\alpha_{11}, \alpha_{12} \dots, \alpha_{NM_N})$. Then, from Section 2.3, $\text{cov} [\tilde{\boldsymbol{\alpha}}] = \mathbf{K}$. Denote $\boldsymbol{\Psi}_j \in \mathbb{R}^{n \times M_j}$ as the the data matrix of the eigenfunctions of \mathbf{C}_{jj} , i.e., the k, ℓ -th element of $\boldsymbol{\Psi}_j$ is the ℓ -th eigenfunction evaluated at \mathbf{s}_k . Then, define the block matrix $\boldsymbol{\Omega}$, where the j, j -th block is $\boldsymbol{\Psi}_j$ and the j, k -th block is the zero matrix of equivalent order for $j \neq k$. Then, we have $\mathbf{Y} \approx \boldsymbol{\Omega} \tilde{\boldsymbol{\alpha}}$, where the approximation is due to the truncation in the univariate KLEs.

Now, perform an eigendecomposition of \mathbf{K} as $\mathbf{K} = \mathbf{E} \boldsymbol{\Lambda} \mathbf{E}^\top$. Then, it is straightforward to see that $\mathbf{E}^\top \tilde{\boldsymbol{\alpha}}$ has variance $\boldsymbol{\Lambda}$. Similarly, $\boldsymbol{\Omega} \mathbf{E}$ also contains orthonormal basis functions since the orthonormality of matrices is preserved under multiplication. Now, collecting the terms of $\boldsymbol{\Omega} \mathbf{E}$ as in Equations (3) and (4), we get the vector-valued eigenfunctions from the univariate processes. Interested readers can also see Cho et al. (2013); Happ and Greven (2018) for a detailed proof and the proof in the opposite direction.

Appendix B Proofs of Propositions 2.1 – 2.5

B.1 Proof of Proposition 2.1

$$\begin{aligned} \text{cov} [\mathbf{y}^A(\mathcal{A}), \mathbf{y}^A(\mathcal{B})] &= \text{cov} \left[\frac{1}{|\mathcal{A}|} \int_{\mathbf{s} \in \mathcal{A}} \mathbf{y}(\mathbf{s}) \, d\mathbf{s}, \frac{1}{|\mathcal{B}|} \int_{\mathbf{r} \in \mathcal{B}} \mathbf{y}(\mathbf{r}) \, d\mathbf{r} \right] \\ &= \frac{1}{|\mathcal{A}|} \frac{1}{|\mathcal{B}|} \int_{\mathbf{s} \in \mathcal{A}} \int_{\mathbf{r} \in \mathcal{B}} \text{cov} [\mathbf{y}(\mathbf{s}), \mathbf{y}(\mathbf{r})] \, d\mathbf{s} \, d\mathbf{r} \\ &= \frac{1}{|\mathcal{A}|} \frac{1}{|\mathcal{B}|} \int_{\mathbf{s} \in \mathcal{A}} \int_{\mathbf{r} \in \mathcal{B}} \mathbf{y}(\mathbf{s}) \mathbf{y}(\mathbf{r})^\top \, d\mathbf{s} \, d\mathbf{r}. \end{aligned}$$

B.2 Proof of Proposition 2.2

We see that from the covariance kernel, we have

$$\begin{aligned}
\text{cov} [\mathbf{y}^A(\mathcal{A}), \mathbf{y}^A(\mathcal{B})] &= \frac{1}{|\mathcal{A}|} \frac{1}{|\mathcal{B}|} \int_{\mathbf{s} \in \mathcal{A}} \int_{\mathbf{r} \in \mathcal{B}} \text{cov} [\mathbf{y}(\mathbf{s}), \mathbf{y}(\mathbf{r})] d\mathbf{s} d\mathbf{r} \\
&= \frac{1}{|\mathcal{A}|} \frac{1}{|\mathcal{B}|} \int_{\mathbf{s} \in \mathcal{A}} \int_{\mathbf{r} \in \mathcal{B}} \mathbb{E}[\mathbf{y}(\mathbf{s})\mathbf{y}(\mathbf{r})^\top] d\mathbf{s} d\mathbf{r} \\
&= \frac{1}{|\mathcal{A}|} \frac{1}{|\mathcal{B}|} \int_{\mathbf{s} \in \mathcal{A}} \int_{\mathbf{r} \in \mathcal{B}} \mathbb{E} \left[\left(\sum_{k=1}^{\infty} \alpha_k \boldsymbol{\psi}_k(\mathbf{s}) \right) \left(\sum_{\ell=1}^{\infty} \alpha_\ell \boldsymbol{\psi}_\ell(\mathbf{r}) \right)^\top \right] d\mathbf{s} d\mathbf{r} \\
&= \sum_{k=1}^{\infty} \sum_{\ell=1}^{\infty} \mathbb{E}[\alpha_k \alpha_\ell] \frac{1}{|\mathcal{A}|} \int_{\mathbf{s} \in \mathcal{A}} \boldsymbol{\psi}_k(\mathbf{s}) d\mathbf{s} \frac{1}{|\mathcal{B}|} \int_{\mathbf{r} \in \mathcal{B}} \boldsymbol{\psi}_\ell(\mathbf{r})^\top d\mathbf{r} \\
&= \sum_{k=1}^{\infty} \sum_{\ell=1}^{\infty} \mathbb{E}[\alpha_k \alpha_\ell] \boldsymbol{\psi}_k^A(\mathcal{A}) \boldsymbol{\psi}_\ell^A(\mathcal{B})^\top \\
&= \sum_{k=1}^{\infty} \lambda_k \boldsymbol{\psi}_k^A(\mathcal{A}) \boldsymbol{\psi}_k^A(\mathcal{B})^\top.
\end{aligned}$$

B.3 Proof of Proposition 2.3

Using Proposition 2.2, it follows that

$$\begin{aligned}
\mathbf{y}^A(\mathcal{A}) &= \frac{1}{|\mathcal{A}|} \int_{\mathbf{s} \in \mathcal{A}} \mathbf{y}(\mathbf{s}) d\mathbf{s} \\
&= \frac{1}{|\mathcal{A}|} \int_{\mathbf{s} \in \mathcal{A}} \sum_{k=1}^{\infty} \alpha_k \boldsymbol{\psi}_k(\mathbf{s}) d\mathbf{s} \\
&= \sum_{k=1}^{\infty} \alpha_k \frac{1}{|\mathcal{A}|} \int_{\mathbf{s} \in \mathcal{A}} \boldsymbol{\psi}_k(\mathbf{s}) d\mathbf{s} \\
&= \sum_{k=1}^{\infty} \alpha_k \boldsymbol{\psi}_k^A(\mathcal{A}).
\end{aligned}$$

B.4 Proof of Proposition 2.4

First, we show that if each of the point-level and areal-level eigenfunctions MKLE (i.e., $\boldsymbol{\psi}(\mathbf{s})$ and $\boldsymbol{\psi}^A$) of $\mathbf{y}(\cdot)$ are the same almost surely (a.s.) over any areal domain \mathcal{A} , the point and areal versions are equal almost surely over the domain, i.e., we want to show that $\mathbf{y}(\mathbf{s}) \stackrel{\text{a.s.}}{=} \mathbf{y}^A(\mathcal{A})$ for $\mathbf{s} \in \mathcal{A}$.

Using Chebyshev's inequality, the following holds

$$\begin{aligned}
\mathbb{P}\left[|\mathbf{y}(\mathbf{s}) - \mathbf{y}^A(\mathbf{s})| > \epsilon\right] &< \frac{1}{\epsilon^2} \mathbb{E}[|\mathbf{y}(\mathbf{s}) - \mathbf{y}^A(\mathbf{s})|^2] \\
&= \frac{1}{\epsilon^2} \mathbb{E}\left[\sum_{k=1}^{\infty} \lambda_k \{\boldsymbol{\psi}_k(\mathbf{s}) - \boldsymbol{\psi}_k^A(\mathbf{s})\}^2\right] \\
&= \frac{1}{\epsilon^2} \sum_{k=1}^{\infty} \lambda_k \mathbb{E}\left[\{\boldsymbol{\psi}_k(\mathbf{s}) - \boldsymbol{\psi}_k^A(\mathbf{s})\}^2\right] \\
&\leq \frac{1}{\epsilon^2} \sum_{k=1}^{\infty} \lambda_k \left[\frac{\delta}{\lambda_k} \mathbb{P}\left[\{\boldsymbol{\psi}_k(\mathbf{s}) - \boldsymbol{\psi}_k^A(\mathbf{s})\}^2 \leq \frac{\delta}{\lambda_k}\right] + \int \{\boldsymbol{\psi}_k(\mathbf{s}) - \boldsymbol{\psi}_k^A(\mathbf{s})\}^2 \mathbb{P}\left[\{\boldsymbol{\psi}_k(\mathbf{s}) - \boldsymbol{\psi}_k^A(\mathbf{s})\}^2 \geq \frac{\delta}{\lambda_k}\right] ds\right].
\end{aligned}$$

Since each $\boldsymbol{\psi}_k(\mathbf{s}) \stackrel{a.s.}{=} \boldsymbol{\psi}_k^A(\mathcal{A})$, the probability in the second term is 0 for any $\delta > 0$. Now, letting $\delta \rightarrow 0$, the first term approaches 0 and hence yields that $\mathbf{y}(\mathbf{s}) \stackrel{a.s.}{=} \mathbf{y}^A(\mathcal{A})$. Applying the *continuous mapping theorem* on \mathbf{y} yields that $\mathbf{f}(\mathbf{y}) \stackrel{a.s.}{=} \mathbf{f}(\mathbf{y}^A)$.

The reverse direction of this theorem can be proven by setting $\mathbf{f}(\mathbf{y}) = \mathbf{y}$ as follows

$$\begin{aligned}
&\mathbf{y}(\mathbf{s}) \stackrel{a.s.}{=} \mathbf{y}^A(\mathcal{A}) \\
&\Rightarrow \mathbf{y}(\mathbf{s}) \alpha_k \stackrel{a.s.}{=} \mathbf{y}^A(\mathcal{A}) \alpha_k \\
&\Rightarrow \mathbf{y}(\mathbf{s}) \int_{\mathbf{r}} \mathbf{y}(\mathbf{r})^\top \boldsymbol{\psi}_k(\mathbf{r}) d\mathbf{r} \stackrel{a.s.}{=} \mathbf{y}^A(\mathcal{A}) \int_{\mathbf{r}} \mathbf{y}(\mathbf{r})^\top \boldsymbol{\psi}_k(\mathbf{r}) d\mathbf{r} \\
&\Rightarrow \int_{\mathbf{r}} \mathbf{y}(\mathbf{s}) \mathbf{y}(\mathbf{r})^\top \boldsymbol{\psi}_k(\mathbf{r}) d\mathbf{r} \stackrel{a.s.}{=} \frac{1}{|\mathcal{A}|} \int_{\mathbf{s} \in \mathcal{A}} \int_{\mathbf{r}} \mathbf{y}(\mathbf{s}) \mathbf{y}(\mathbf{r})^\top \boldsymbol{\psi}_k(\mathbf{r}) d\mathbf{r} d\mathbf{s} \\
&\Rightarrow \int_{\mathbf{r}} \mathbb{C}(\mathbf{s}, \mathbf{r}) \boldsymbol{\psi}_k(\mathbf{r}) d\mathbf{r} \stackrel{a.s.}{=} \frac{1}{|\mathcal{A}|} \int_{\mathbf{s} \in \mathcal{A}} \int_{\mathbf{r}} \mathbb{C}(\mathbf{s}, \mathbf{r}) \boldsymbol{\psi}_k(\mathbf{r}) d\mathbf{r} d\mathbf{s} \\
&\Rightarrow \boldsymbol{\psi}_k(\mathbf{s}) \stackrel{a.s.}{=} \frac{1}{|\mathcal{A}|} \int_{\mathbf{s} \in \mathcal{A}} \boldsymbol{\psi}_k(\mathbf{s}) d\mathbf{s} \quad (\text{From Equation (2)}) \\
&\Rightarrow \boldsymbol{\psi}_k(\mathbf{s}) \stackrel{a.s.}{=} \boldsymbol{\psi}_k^A(\mathcal{A}).
\end{aligned}$$

This concludes the equivalence of the two sides of the Proposition 2.4.

B.5 Proof of Proposition 2.5

Recall that,

$$\begin{aligned}\text{cov}(\mathbf{y}(\mathbf{s}), \mathbf{y}(\mathbf{s})) &= \sum_{k=1}^{\infty} \lambda_k \boldsymbol{\psi}_k(\mathbf{s}) \boldsymbol{\psi}_k(\mathbf{s})^\top, \\ \text{cov}(\mathbf{y}^A(\mathcal{A}), \mathbf{y}^A(\mathcal{A})) &= \sum_{k=1}^{\infty} \lambda_k \boldsymbol{\psi}_k^A(\mathcal{A}) \boldsymbol{\psi}_k^A(\mathcal{A})^\top.\end{aligned}$$

Similarly, we can derive the following

$$\begin{aligned}\text{cov}(\mathbf{y}(\mathbf{s}), \mathbf{y}^A(\mathcal{A})) &= \frac{1}{|\mathcal{A}|} \int_{\mathbf{r} \in \mathcal{A}} \text{cov}(\mathbf{y}(\mathbf{s}), \mathbf{y}(\mathbf{r})) d\mathbf{r} \\ &= \frac{1}{|\mathcal{A}|} \int_{\mathbf{r} \in \mathcal{A}} \sum_{k=1}^{\infty} \lambda_k \boldsymbol{\psi}_k(\mathbf{s}) \boldsymbol{\psi}_k^\top(\mathbf{r}) d\mathbf{r} \\ &= \sum_{k=1}^{\infty} \lambda_k \boldsymbol{\psi}_k(\mathbf{s}) \frac{1}{|\mathcal{A}|} \int_{\mathbf{r} \in \mathcal{A}} \boldsymbol{\psi}_k^\top(\mathbf{r}) d\mathbf{r} \\ &= \sum_{k=1}^{\infty} \lambda_k \boldsymbol{\psi}_k(\mathbf{s}) \boldsymbol{\psi}_k^A(\mathcal{A})^\top.\end{aligned}$$

Now,

$$\begin{aligned}\sum_{k=1}^{\infty} \lambda_k \boldsymbol{\psi}_k^\top(\mathbf{s}) \boldsymbol{\psi}_k(\mathbf{s}) &= \text{trace} \left(\sum_{k=1}^{\infty} \lambda_k \boldsymbol{\psi}_k^\top(\mathbf{s}) \boldsymbol{\psi}_k(\mathbf{s}) \right) \\ &= \text{trace} \left(\sum_{k=1}^{\infty} \lambda_k \boldsymbol{\psi}_k(\mathbf{s}) \boldsymbol{\psi}_k(\mathbf{s})^\top \right) \\ &= \text{trace}(\text{cov}(\mathbf{y}(\mathbf{s}))).\end{aligned}$$

Similarly, $\sum_{k=1}^{\infty} \lambda_k \boldsymbol{\psi}_k^A(\mathcal{A})^\top \boldsymbol{\psi}_k^A(\mathcal{A}) = \text{trace}(\text{cov}(\mathbf{y}^A(\mathcal{A})))$. Then, under the squared-error loss, the MVCAGE loss becomes

$$\begin{aligned}MVCAGE(\mathcal{A}) &= \frac{1}{|\mathcal{A}|} \int_{\mathbf{s} \in \mathcal{A}} \sum_{k=1}^{\infty} \lambda_k \left[\boldsymbol{\psi}_k^A(\mathcal{A}) - \boldsymbol{\psi}_k(\mathbf{s}) \right]^\top \left[\boldsymbol{\psi}_k^A(\mathcal{A}) - \boldsymbol{\psi}_k(\mathbf{s}) \right] d\mathbf{s} \\ &= \sum_{k=1}^{\infty} \lambda_k \frac{1}{|\mathcal{A}|} \int_{\mathbf{s} \in \mathcal{A}} \left[\boldsymbol{\psi}_k^\top(\mathbf{s}) \boldsymbol{\psi}_k(\mathbf{s}) - 2\boldsymbol{\psi}_k^\top(\mathbf{s}) \boldsymbol{\psi}_k^A(\mathcal{A}) + \boldsymbol{\psi}_k^A(\mathcal{A})^\top \boldsymbol{\psi}_k^A(\mathcal{A}) \right] d\mathbf{s} \\ &= \frac{1}{|\mathcal{A}|} \int_{\mathbf{s} \in \mathcal{A}} \text{trace} \left[\text{cov}(\mathbf{y}(\mathbf{s}), \mathbf{y}(\mathbf{s})) - 2\text{cov}(\mathbf{y}(\mathbf{s}), \mathbf{y}^A(\mathcal{A})) + \text{cov}(\mathbf{y}^A(\mathcal{A}), \mathbf{y}^A(\mathcal{A})) \right] d\mathbf{s}\end{aligned}$$

$$\begin{aligned}
&= \frac{1}{|\mathcal{A}|} \int_{\mathbf{s} \in \mathcal{A}} \text{trace} \left[\text{cov} \left(\mathbf{y}(\mathbf{s}) - \mathbf{y}^A(\mathcal{A}), \mathbf{y}(\mathbf{s}) - \mathbf{y}^A(\mathcal{A}) \right) \right] d\mathbf{s} \\
&= \frac{1}{|\mathcal{A}|} \int_{\mathbf{s} \in \mathcal{A}} \text{trace} \mathbb{E} \left[\left(\mathbf{y}(\mathbf{s}) - \mathbf{y}^A(\mathcal{A}) \right) \left(\mathbf{y}(\mathbf{s}) - \mathbf{y}^A(\mathcal{A}) \right)^\top \right] d\mathbf{s}.
\end{aligned}$$

The other part follows straightforwardly by noting that $\text{cov}(\mathbf{y}(\mathbf{s}), \mathbf{y}^A(\mathcal{A})) = \frac{1}{|\mathcal{A}|} \int_{\mathbf{r} \in \mathcal{A}} \text{cov}(\mathbf{y}(\mathbf{s}), \mathbf{y}(\mathbf{r})) d\mathbf{r}$.

Appendix C Block Gibbs Sampling for the MVOC Model

Denote $\widehat{\boldsymbol{\nu}}_j$ as the ordinary least-square estimate with $Z_j(\mathbf{s})$ as response and $\phi_{jk}(\mathbf{s})$ as predictor. Denote its k -th element as $\widehat{\nu}_{jk}$. Also denote the g -sum of square as $\text{SSR}_j = \sum_{i=1}^n [Z_j(\mathbf{s}_i) - \mu_j - \sum_{k=1}^{M_j} \frac{g}{g+1} \phi_{jk}(\mathbf{s}_i) \widehat{\nu}_{jk}]^2$. Then, one can draw posterior samples of the hyperparameters using a block Gibbs sampler, where the hyperparameters are sequentially sampled from each of their specific full conditional distributions as follows

$$\begin{aligned}
\pi(\mu_j | \cdot) &\sim \mathcal{N} \left(\frac{1}{n} \sum_{k=1}^n [Z_j(\mathbf{s}_i) - \sum_{k=1}^{M_j} \frac{g}{g+1} \phi_{jk}(\mathbf{s}_i) \widehat{\nu}_{jk}], \frac{\sigma_j^2}{n} \right), \\
\pi(\sigma_j^2 | \cdot) &\sim \text{Inverse Gamma} \left(\frac{n}{2}, \frac{\text{SSR}_j}{2} \right), \\
\pi(\boldsymbol{\nu}_j | \cdot) &\sim \mathcal{N} \left(\frac{g}{g+1} \widehat{\boldsymbol{\nu}}_j, \frac{g}{g+1} \sigma_j^2 (\boldsymbol{\Phi}_j^\top \boldsymbol{\Phi}_j)^{-1} \right).
\end{aligned}$$

One first samples from the full conditional distribution $\pi(\sigma_j^2 | \mathbf{Y})$. Then, conditioned on the sampled σ_j^2 , we can draw samples of μ_j and $\boldsymbol{\nu}_j$ from their conditional distributions. Then, using Monte Carlo integration, we can integrate out μ_j and σ_j^2 to get $\pi(\boldsymbol{\nu}_j | \mathbf{Y})$.

Appendix D MKLE Construction from MVOC basis

Note that $\text{cov}(\mathbf{y}^{\text{vec}}) = \mathbf{C} = \boldsymbol{\Phi} \text{cov}(\boldsymbol{\nu}^{\text{vec}}, \boldsymbol{\nu}^{\text{vec}}) \boldsymbol{\Phi}^\top = \boldsymbol{\Phi} \mathbf{K} \boldsymbol{\Phi}^\top$. Now, use the prior information on the model parameters to estimate \mathbf{K} as $\widehat{\mathbf{K}}$. Since $\boldsymbol{\Phi}$ is orthonormal, it is closed under multiplication by another orthonormal matrix. Similar to the derivation in Section 2.3, we need to find the orthonormal matrix that decorrelates \mathbf{K} . We decompose $\widehat{\mathbf{K}}$ as $\mathbf{K} = \mathbf{E} \boldsymbol{\Lambda} \mathbf{E}^\top$. Then, applying the

Proposition 5 from (Happ and Greven, 2018) and using the same arguments from Appendix A, it is straightforward to see that the eigenvalues Λ are the eigenvalues of the MKLE. Similarly, the constructed eigenfunctions and expansion coefficients in ((11)) satisfy the properties of the multivariate eigenfunctions of the MKLE.

Appendix E Prediction of Ocean Color

We apply our methodology to perform a bivariate aggregation in the coastal Gulf of Alaska (Leeds et al., 2014; Wikle et al., 2013) based on the satellite data of ocean color and ROMS ocean model (Regional Ocean Modeling System) (Haidvogel et al., 2010) output for the amount of chlorophyll. There are many satellites focused on the collection of ocean color datasets, e.g., SeaWiFS, MODIS, MERIS, etc. Ocean color provides information on the quantity of phytoplankton on the ocean surface. Therefore, it leads to the inference of the primary productivity and ecology of the upper levels of the ocean. Moreover, the measurement of chlorophyll is another important covariate correlated with species distribution and ocean ecology through its fundamental role as a food source in the lower levels of the food chain. ROMS is a three-dimensional (in space) ocean circulation model that simulates oceanic and estuarine processes at regional scale over time. The model can be used to simulate water temperature, salinity, currents, and other physical and biogeochemical variables, including chlorophyll content. Therefore, we consider a spatial aggregation or regionalization based on the joint distribution of ocean color from the SeaWiFS satellite and ROMS ocean model output for chlorophyll.

We consider the data from 12 May 2000, which has complete observations at 4718 spatial coordinates. We use the LMC method from Section 3.3 here to estimate the joint covariance matrix with the bivariate Matérn kernel. Then, we applied our two-stage regionalization algorithm to minimize the value of the MVCAGE statistic. Figure 5 shows the results of using our approach

on these data. We choose the lower and upper bounds to be 250 and 350 and note that the regionalization with 306 areal regions had the minimum amount of MVCAGE. Hence, this is an order-of-magnitude reduced representation of the original data in the aggregated scale such that the amount of ecological fallacy in the aggregation is minimized.

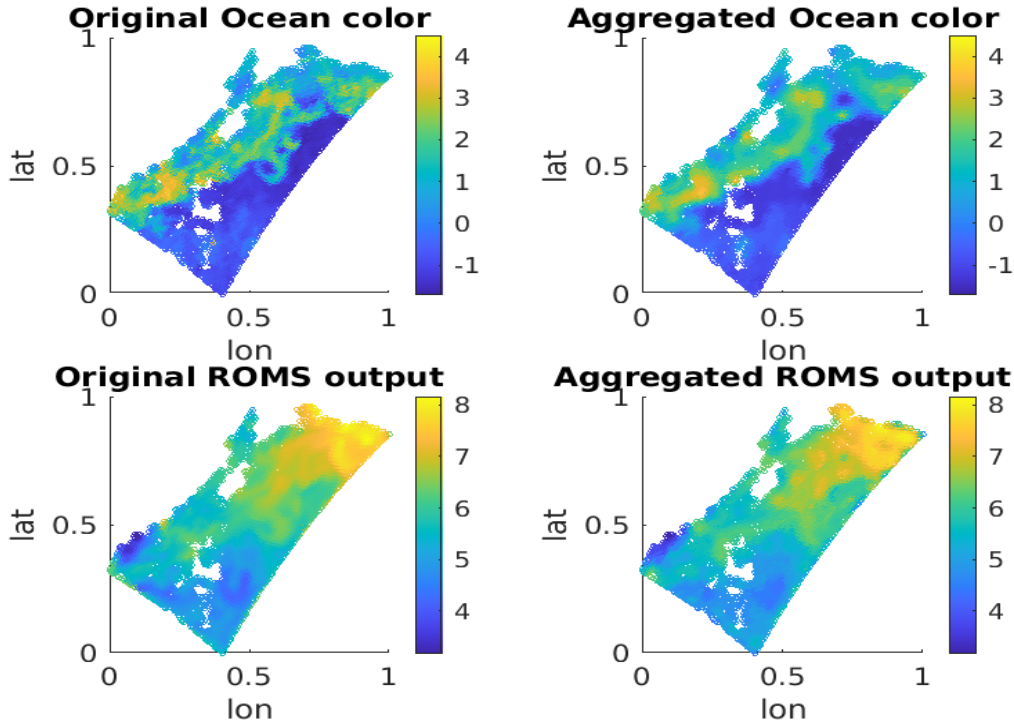


Figure 5: **Regionalization of Ocean Color and ROMS Model Output:** We applied our methodology to aggregate the SeaWiFS ocean color data which is an indicator of the presence of chlorophyll. The top row shows the point level (left) and the areal level (right) aggregation of the observed ocean color. The bottom row demonstrates the same for the ROMS ocean model output for the amount of chlorophyll.

Appendix F Univariate KLE Computation Details

Recall that $C_{jj} \in \mathbb{R}^{n \times n}$ is the covariance matrix with k, ℓ -th element as $C_{jj}(s_k, s_\ell) = \text{cov} [y_j(s_k), y_j(s_\ell)]$.

Also recall that the eigenfunctions and eigenvalues of C_{jj} are $\{\psi_{j1}, \psi_{j2}, \dots\}$ and $\{\lambda_{j1} \geq \lambda_{j2} \geq \dots\}$.

For the functional eigendecomposition of C_{jj} , the Galerkin method uses some orthonormal basis functions denoted as $\phi_{j1}, \dots, \phi_{j\widetilde{M}_j}$.

We denote the data matrix version of the orthonormal basis functions as $\Phi_j \in \mathbb{R}^{n \times \widetilde{M}_j}$, where the i, k -th element is given by $\phi_{jk}(\mathbf{s}_i)$. Similarly, define Ψ_j is the matrix with elements $\psi_{jk}(\mathbf{s}_i)$. In the Galerkin method, we assume that the orthonormal bases $\{\phi_{jk}\}_{k=1}^{\widetilde{M}_j}$ span the eigenfunctions $\{\psi_{jk}\}_{k=1}^{M_j}$, i.e., $\Psi_j = \Phi_j \mathbf{F}_j$. To compute \mathbf{F}_j , we use the Fredholm integral equation that yields the following

$$\begin{aligned} \int_{\mathbf{s}} \mathbf{C}_{jj}(\mathbf{s}, \mathbf{r}) \psi_{jk}(\mathbf{s}) d\mathbf{s} &= \lambda_{jk} \psi_{jk}(\mathbf{r}) \\ \Rightarrow (\mathbf{F}_j)^\top \int_{\mathbf{s}} \mathbf{C}_{jj}(\mathbf{s}, \mathbf{r}) \phi_{jk}(\mathbf{r}) d\mathbf{s} &= (\mathbf{F}_j)^\top \lambda_{jk} \psi_{jk}(\mathbf{r}) \\ \Rightarrow (\mathbf{F}_j)^\top \int_{\mathbf{s}} \int_{\mathbf{r}} \mathbf{C}_{jj}(\mathbf{s}, \mathbf{r}) \phi_{jk}(\mathbf{s}) \phi_{j\ell}(\mathbf{r}) d\mathbf{s} d\mathbf{r} &= (\mathbf{F}_j)^\top \lambda_{jk} \int_{\mathbf{r}} \phi_{jk}(\mathbf{r}) \phi_{j\ell}(\mathbf{r}) d\mathbf{r}. \end{aligned}$$

Define \mathbf{U}_j with k, ℓ -th element $\int_{\mathbf{s}} \int_{\mathbf{r}} \mathbf{C}_{jj}(\mathbf{s}, \mathbf{r}) \phi_{jk}(\mathbf{s}) \phi_{j\ell}(\mathbf{r}) d\mathbf{s} d\mathbf{r}$. Also, denote Λ_j as the diagonal matrix with diagonals λ_{jk} . Then in matrix form, the above equation becomes $\mathbf{U}_j \mathbf{F}_j = \mathbf{F}_j \Lambda_j$. This is the same as the generalized eigenvalue problem, i.e., the solution sets \mathbf{F}_j and Λ_j are the eigenvectors and eigenvalues of \mathbf{U}_j . This implies that the k -th eigenvalue of C_{jj} is the k -th diagonal element of Λ_j . Similarly, the k -th eigenfunction is obtained by post-multiplying the k -th column of \mathbf{F}_j by Φ_j .